1-1-2014

Quantifying Human Impacts on River Bar Morphology Using Digital Photogrammetry

Aaron Zettler-Mann
University of Denver

QUANTIFYING HUMAN IMPACTS ON RIVER BAR MORPHOLOGY USING DIGITAL PHOTOGRAMMETRY

_____

A Thesis

Presented to

The Faculty of Natural Science and Mathematics

University of Denver

_____

In Partial Fulfillment

of the Requirements for the Degree

Master of Arts

_____

by

Aaron Zettler-Mann

November 2014

Advisor: Dr. J. Michael Daniels

Author: Aaron Zettler-Mann
Title: QUANTIFYING HUMAN IMPACTS ON RIVER BAR MORPHOLOGY USING DIGITAL PHOTOGRAMMETRY
Advisor: Dr. J. Michael Daniels
Degree Date: November 2014

Abstract

Historically, the study of fluvial geomorphology has been dominated by the field method of surveying using a level and surveying rod. Beginning in the 1980s, the use of ground based and aerial LiDAR increased in popularity as a surveying method. However, LIDAR is expensive and requires significant training to operate. In recent years there has been an increase in the applicability of digital photogrammetry in the field of fluvial geomorphology. Lower costs, streamlined training and an increased accuracy all make digital photogrammetry a promising tool for the field geomorphologist. A study of the morphologic changes of four river bars on the Browns Canyon section of the Arkansas River, Colorado is used to explore the potential of digital photogrammetry by attempting to quantify the impacts of recreation river users on bar morphology. By creating high resolution digital elevation models (DEMs) at time intervals from 24 hours to several days, DEMs of difference (DoDs) were created and analyzed using the open-source 3D data processing software CloudCompare. DoDs were correlated with historical, daily commercial river user data to derive a relationship. Verification concerning the validity of CloudCompare was done using a simple experiment simulating erosion and deposition of a known volume of material.

Table of Contents

Figures

Chapter One: Introduction

Over eight years working as a raft guide on rivers throughout California, I consistently noticed a change in the shape and extent of sand bars that were most popular for lunch stops. Throughout the season, sand bars became smaller, and the angle of the water-bar interface became shallower. Recent technological improvements in digital elevation model generation and geomorphologic change detection have created the opportunity to quantify this change.

One such technological advance is digital photogrammetry, more generally referred to structure-from-motion (SfM). The use of SfM in geomorphology has become increasingly popular in recent years as technology has improved (Lane, 2000; Lane et al., 1993: Bird et al., 2010; Chandler et al., 2002; Barker et al., 1997; Marcus & Fonstad, 2010). Within the last decade, advances in digital technology and decreases in equipment costs have enabled the use of digital photogrammetry specifically over a wide range of applications, and at higher resolutions (Matthews et al., 2004). One increasingly common application is in the study of fluvial geomorphology. Digital photogrammetry also allows erosion and deposition data to be easily quantified. This gives it a distinct advantage when calculating sediment budgets (Heritage et al., 1998). There are especially noticeable advantages to this technique for river bar morphology where change occurs rapidly, such as braided rivers (Chandler et al., 2002). Carbonneau et al., (2003) and Westoby et al., (2012) discuss the high degree of precision possible as well.

Additionally, digital photogrammetry offers a low cost and easy-to-learn approach to high resolution digital elevation model generation, especially when compared to alternative methods such as LiDAR. The equipment required for digital photogrammetry is also more compact and can be operated by one person.

Using digital photogrammetry, this study will describe morphologic change on four river bars on the Browns Canyon section of the Arkansas River. Morphologic change over the duration of the four month study period will be quantified and correlated with historical average daily river user numbers. Fluctuations in discharge, bar sediment composition and rainfall will also be taken into consideration. The null and alternate hypotheses for all of the river bars are:

H_0: There is no morphologic change during the study period.
H_{A1}: There is morphologic change due to human impacts.
H_{A2}: There is morphologic change due to climatic factors.
H_{A3}: There is morphologic changes due to unknown factors.

Conceptual Background for Digital Photogrammetry

Structure-from-Motion

Structure-from-Motion (SfM) is the general term for optically derived digital surface generation. The process for generating the surface relies on the matching of pixels by the SfM software, based on color from multiple stereoscopically overlapping photographs. As outlined by Westoby et al., (2012) and Matthews (2008), the first step is identification by the software of many invariate points. An invariate point is one which is visible in three or more photographs and is constantly identifiable regardless of factors such as camera position and changes in lighting. The number of invariate points in a

project will vary based on the size of the project. For large projects on the order of tens of meters square (such as this project), hundreds of invariate points are identified by the software. After placing the invariate points in a relative 3D space, additional pixels are matched and placed in space based on their relationship to the invariate points. The stereoscopic overlap of the photos within a photo set allows the software to place aligned pixels in a relative X, Y, Z coordinate system. This process is similar to the triangulation method that satellites use to position a GPS unit.

The use of SfM techniques in the study of geomorphology has become increasingly popular in recent years as technology has improved (Lane, 2000; Bird et al., 2010; Chandler et al., 2002; Barker et al., 1997; Marcus & Fonstad, 2010). Within the last decade, advances in digital technology and decreases in equipment costs have prompted an increase in the use of digital photogrammetry specifically, over a wide range of applications and at higher resolutions (Matthews et al., 2008).

One of the earliest applications of modern photogrammetry was by Barker et al. (1996) using an analytical stereoplotter to mathematically solve for point placement between stereoscopically overlapping photographs. When compared to previous methods using mechanical point placement, this novel point placement solution allowed for greater accuracy and more variability in the types of data that could be derived. Using film cameras, Barker et al. (1996) effectively and accurately captured bar morphology. Their paper represents a new way of matching and placing point pairs and lays the groundwork for the digital photogrammetry in the future. A later paper by Heritage et al. (1998) is one of the earliest to point to the value of photogrammetry in the study of geomorphology, acknowledging that the detail possible far exceeds that of the alternative

methods. They also attribute the increase in detail to the ability to mathematically resolve point placement.

Beginning in the early 2000's digital photogrammetry began to gain popularity. Lane, (2000) reviews digital photogrammetry in the study of fluvial geomorphology. Relying on works such as Barker et al. (1996) and Heritage et al. (1998), Lane (2000) recognized the increase in applicability of photogrammetry in fluvial settings with improvements in digital technology. Lane (2000) also goes on to describe new problems associated with digital photogrammetry, many of which are discussed in section 1.2. Despite the challenges associated with a developing method, digital photogrammetry offers low cost and highly detailed DEM generation in fluvial settings.

Through the 2000's, as digital camera technology improved and digital photogrammetry techniques were refined, the frequency of use in the study of fluvial settings increased. The result was many river reach scale surveys using both terrestrial and aerial picture acquisition, in increasingly complicated topographic settings (Charbonneau et al., 2001; Chandler et al., 2002; Bird et al., 2010; Marcus and Fonstad, 2010; Fonstad et al., 2012; Westoby et al., 2012; Lague et al., 2013). This sample of studies helps illustrate the increase in proliferation of digital photogrammetry when studying fluvial settings. Of notable informative relevance to the present work are Marcus and Fonstad (2010) and Fonstad et al. (2012).

Marcus and Fonstad (2010) discuss high resolution, multi-scale topographic surveys from a variety of techniques, including film and digital photogrammetry as well as LiDAR. They address the proliferation of studies and increasing accuracy of digital photogrammetry in generating high resolution DEMs. This paper recognizes the

beginnings of remote sensing to study fluvial settings in the 1990's and looks forward to the increasing accuracy offered by digital photogrammetry and LiDAR in the study of fluvial geomorphology. Marcus and Fonstad (2010) also note the benefit of digital photogrammetry as a cost efficient alternative to LiDAR when creating high resolution DEMs.

A later paper by Fonstad et al., (2012) compares digital photogrammetry to LiDAR. This paper uses repeat surveys by both techniques in the same fluvial landscape. The authors find that both techniques are capable of developing similarly accurate DEMs. Through this paper and others like it, digital photogrammetry is validated as an alternative method for generating high resolution DEMs.

My work builds on the body of work using remote sensing techniques to study fluvial geomorphology. I rely on early fluvial geomorphology studies using photogrammetry and the development and validation of digital photogrammetry in. My work moves beyond many of those studies, focusing on smaller areas and quantifying smaller scale change. Using digital photogrammetry allowed me to quickly and efficiently create high resolution DEMs of river bars and compare then to quantify change during the summer of 2014. While many of the above mentioned papers employ digital photogrammetry to examine change on a river reach scale, I explore the capabilities of digital photogrammetry to capture smaller scale change. This helps illustrate an alternative use for digital photogrammetry in the study of fluvial geomorphology.

Terrestrial based digital photogrammetry allows for high-resolution analysis of changes in channel morphology with considerably less work than traditional survey

methods (Barker et al., 1997). Photogrammetry also allows for the inclusion of bank scour and fill data that are often lost when using traditional surveying techniques. This gives it a distinct advantage when calculating sediment budgets (Heritage et al., 1998). There are especially noticeable advantages to this technique for river bar morphology where change occurs rapidly, such as braided rivers (Chandler et al., 2002). Lane (2000) describes how photogrammetry builds on the traditional survey methods of a rod and surveying level, derived from engineering, offering significant increases in the morphologic detail. He also discusses the benefits of photogrammetry for the ease and accuracy of data acquisition. Matthews (2008) describes additional benefits of photogrammetry for situations where change may only occur in very small quantities.

Challenges Associated with Digital Photogrammetry.

Along with the benefits of photogrammetry in fluvial geomorphology, there are also challenges, as outlined by Lane (2000) and Westoby et al (2012). A balance between detail desired and the processing time needed must be struck. Additionally, higher levels of detail necessitate shorter object-to-camera distances (Matthews, 2008). In larger study areas, this requires significantly more pictures which may lead to prohibitively long processing times (Lane 2000; Matthews, 2008; Westoby et al., 2012). Longer object-to-camera distances aid in decreasing the processing time, but may lead to greater distortion and reduced accuracy (Lane, 2000). Westoby et al., (2012) present the additional consideration when using photogrammetry in the study of fluvial settings, that active river channels often contain water. Because the surface of water is constantly changing, digital photogrammetry is unable to resolve the portion of a picture with water surfaces. The result is that the apparent size of a bar is inversely related to changes in

stage height; as discharge increases, the apparent area of the bar decreases. They also describe the potential for gaps in data when some objects such as landforms in the foreground or vegetation block features in the background. From personal experience, this type of obstruction problem can be solved by varying the camera location.

Matthews (2008) defines close range photogrammetry as any project where the object-to-camera distance is 300 meters or less. As the object-to-camera distance gets shorter (approximately one meter), resolutions of 0.025 mm are possible. Based on the high level of potential precision, close range photogrammetry has the ability to detect small changes in deposition and erosion (Matthews, 2008). Carbonneau et al., (2003) and Westoby et al., (2012) discuss the high degree of precision possible as well. They also extol the relative ease and low cost with which highly precise DEMs are possible, even with poor camera calibration and for relatively inexperienced photogrammetrists.

Review of Relevant Literature

The following section reviews fluvial geomorphology to better contextualize morphologic variability in river bars. Channel characterization, entrainment and deposition are all summarized as a foundation for natural channel morphology. I also review the literature on recreation and river bars as well as the impacts of foot traffic on erosion in general, and cattle on bar morphology. This provides a conceptual framework for my research on human induced river bar morphology. I end with a discussion of error in digital photogrammetry generally, correcting error in photogrammetry using PhotoScan, and the analytical software CloudCompare.

Channel Characterization

Channel form and location are a function of discharge, the quantity and quality of entrained sediment and the character of the geology that makes up the bed and banks of the channel (Leopold et al., 1964). Variability in some or all of the above factors can result in a large diversity in channel cross-section shape, and reach-scale form, potentially many times within a river's length. The resulting diversity in theoretical channel form has led to challenges in the development of a comprehensive channel classification scheme.

The process of characterizing channels is complicated due to the inherent diversity associated with variability of river morphology. Knighton (1998) synthesized a means of classification based on a characteristic that seems to play the most significant role in predicting channel form; boundary composition. In this classification scheme, the stream boundary is first classified as either cohesive (A) or non-cohesive (B). Within these two categories, the character of the stream boundary is further classified as either a bedrock channel (A1) or silt-clay channel (A2), or a sand-bed channel (B1), gravel-bed channel (B2) or boulder-bed channel (B3). Additional classification is possible based on other criteria such as sinuosity, depth ratio and channel slope; all of which create a more detailed picture of the channel in question and increase the descriptive power of the classification scheme. Regardless of the classification scheme used, it is commonly understood that any classification is only applicable on a reach-length scale as the characteristic of a stream change quite rapidly. Most stream channels are non-cohesive material, with gravel and boulder-bed channels being dominant (Knighton, 1998). Many gravel and boulder-bed channels in non-meandering streams display a repeating pattern

of deep pools and shallow riffles that occur at intervals of every 5-7 widths (Leopold et al., 1964). The present study location is a gravel and boulder-bed channel with a pattern of repeating pools and riffles similar to that described by Leopold et al., (1964) and Knighton (1998). For the purposes of this study, I use the terms river bar, bar and beach interchangeably to refer to areas comprised of unconsolidated, depositional material with little to no vegetation.

Entrainment and Deposition

Entrainment of a particle refers to the point when a particle begins to move; that is, when the shear stress of the current is enough to overcome the forces of gravity and friction holding the particle in place. There are two channel characteristics that are important in deciding the relationship between the forces of shear stress, and gravity and friction. They are the size of the clast, and the size of the clast relative to the bed it is laying on. Larger particles require a higher shear stress before mobilization than smaller particles. This means that relatively smaller particles are preferentially mobilized at a given shear stress, leaving the larger particles behind. The size of a clast relative to the surrounding river bed is also an important characteristic in the likelihood of particle mobilization.

In a gravel bed river such as the one being studied, flow paths are always turbulent. Turbulent flow paths are due to the obstacles found in the channel that create resistance. There are three types of resistance found in a channel: skin resistance, internal distortion resistance and spill resistance (Leopold et al., 1964). Skin resistance refers to the resistance from the water-bank interaction and the resulting turbulence. Internal distortion resistance is the resistance associated with distortions of the channel such as

bars, bends and eddies. Spill resistance is an object that disrupts or blocks downstream flow, forcing the channel to go around or over the object, locally decreasing velocity. Fluvial zones that experience spill resistance and skin resistance will often also see flow separation.

Flow separation may be defined as a point along the channel where the downstream flow becomes unstable due to a change in the channel width. This instability causes downstream flow paralleling the bank to break away from the channel boundary, creating a zone where flow paths are different than the main channel. These zones are often referred to as eddies (Leeder & Bridges, 1975). Eddies are separated from the main channel by a narrow, near vertical, area of hydraulic shear where the velocity and direction of flow change rapidly. This is referred to as the eddy line by Rubin et al., (1990). The water on the opposite side of the eddy line from the main channel flows in an upstream direction. The flow path of water within an eddy circulates either clockwise or counter clockwise, depending on the side of the stream it is found (Leeder & Bridges 1975; Leopold et al., 1964). Because flow separation occurs in areas where channel width changes, sudden widening of the channel, meander bends, rocky outcrops and mid channel boulders may all generate zones of flow separation (Leeder and Bridges, 1975; Rubin et al., 1990). Within an eddy, the velocity of the current tends to be lower than that of the main channel. When the shear velocity decreases below the settling velocity of entrained particles, deposition begins to occur (Knighton 1998). The deposition of entrained sediment in zones of flow separation thus leads to the development of river bars (Rubin et al., 1990). Within a river system, bars may change size and location depending on discharge. However, many bars remain relatively stable except during high discharge

events (Vincent and Andrews 2008). Two of the four bars (beach #1 and #3) in my study reach are characterized by deposition associated with widening of the channel at high water events. One is due to a combination of a meander bend and flow separation due to a large, mid channel boulder (beach #2). Beach #4 is the result of a sudden change in channel direction caused by an exposed bedrock cliff on river right.

Vincent and Andrews (2008) describe three main factors that contribute to the formation of river bars; suspended sediment load, variable discharge regime, and locations with recirculating flow. Suspended sediment load refers to the quantity and size of entrained sediment within a channel given a specific discharge. A variable discharge regime describes the need for discharge to vary through time such that particles of various sizes will experience alternately entrainment or deposition. Finally, they characterize the need for variations in the channel width such that flow separation occurs to varying degrees, depending on discharge. Flow separation allows for the deposition of entrained sediment. The Vincent and Andrews (2008) study is mostly concerned with the formation of sand bars suitable for use by recreational river runners. Their findings indicate that, while all three factors play a role in the creation of sandbars, the quantity of suspended sediment is the best predictor of the bar frequency within a river reach.

Related to the formation of river bars within a depositional zone, sorting of clasts by size occurs. This sorting occurs within a given bar and along the river bed and is driven by the shear stress at a given location. Sorting may occur at the point of entrainment, during transport and/or at particle deposition (Powell, 1998). Sorting at entrainment is driven by the ability of the river to move clasts of a specific size. As the discharge increases, large clasts will be mobilized. In this way, there is discharge based

sorting at the point of entrainment. During transport, variation in turbidity within the channel due to bed-form factors may result in the preferential settling or transport of some particles that are near the point of entrainment. Depositional sorting tends to be seen in channel cross section. The methodical decrease in stream velocity at the channel margins leads to general fining of particle sizes. The relationship between these three potential points of sorting is very close, with significant overlap.

Once a clast has passed the threshold for entrainment it is considered entrained, and is transported downstream. The distance downstream it travels is dictated by the turbidity of the river. Turbidity of the current is dictated by the bed surface. There is some evidence to suggest that a particle will settle out of the water column in areas where the bedform is of a similar size to that of the entrained particle (Powell, 1998). This depositional sorting by mean bedform clast size is seen in the riffle-pool organization of many streams. Additionally, variability in turbidity and flowpath within channel will result in sorting tangential to the flow direction. Take a cross section at a meander bed, for example, moving from the thalweg to the point bar. At the thalweg there is an initial fining of the bed due to the relatively low turbidity associated with the deeper channel. Continuing towards the point bar, the bed material becomes coarser, associated with increased levels of turbidity. Moving up onto the point bar, a general fining begins to occur again, attributed to slower speeds and less turbidity of the eddy (Powell, 1998). The general trend of fining of sediment from thalweg to point bar is also observed by Clayton and Pitlick (2007) on meander bends on the Upper Colorado River. They suggest that the differential routing of fine and coarse grain sizes within a cross section promotes mobilization of finer particles. They suggest that the increase in mobilization is

because the finer particles are not hidden by larger particles in deeper areas of the channel.

The deposition of an entrained particle is dictated by a decrease in the turbidity of the stream or decrease in velocity such that the energy needed for transportation is no longer available. In this way, we also see sorting of particles by size. Evidence for depositional sorting is clearest in fluvial settings that are only periodically inundated with water. Examples of this are the fining of sediment moving away from the main channel and the downstream fining of sediment along a given bar (Powell, 1998).

There are additional anthropogenic factors that may induce a profound effect on the erosional and depositional environment of a fluvial system. One of the most important is a dam on the upstream boundary of a river reach. The study location for the present research has two upstream dams. The result of a dam on the bed and bar morphology is a general increase in the mean clast size, referred to as bed armoring. Bed armoring occurs as finer, more easily mobilized clasts are transported downstream, leaving the larger particle sizes. Because dams also decrease maximum discharge levels, the remaining clasts tend to be mobilized less frequently than they would in a natural setting (Petts, 1984). For the current study location, this means that many of the bars in question are comprised of a coarser particle size than may naturally occur.

Recreation and River Bars

Recognition for the need to quantify the impact of human use on river bar morphology developed in the Grand Canyon of the Colorado River. Early work was done by Kaplinski et al., (2003) who explored the history of campsite monitoring for the Grand Canyon. Campsite inventories for this reach of river began in 1975 and occurred

in 1976 and 1984. Beginning in 1991 the Adopt-a-Beach program was introduced. Commercial Grand Canyon river guides volunteered to take pictures of their adopted beach/camp sites throughout the season. Results were then summarized in a series of reports for a single year, and multiple years (Thompson et al., 1997; O'Brian et al., 1999; Thompson, 2001; O'Brian et al., 2000; Thomson 2002). One of the main objectives of the Adopt-a-Beach program was to monitor changes in beach shape and extent due to flood-event-mimicking dam releases. As part of the Adopt-a-Beach program, volunteers noted that during peak use times, many sandbars graded to a gentler slope as a result of human use. Anecdotal evidence from volunteer guides in the Adopt-a-Beach program also noted, "considerable erosion as the season progressed" (Thompson et al., 1997). While not characterized as significant on the Colorado River, the Adopt-a-Beach program does present some evidence that there are noticeable effects on river bars due to human traffic. The reports of human induced erosion from the Adopt-a-Beach program align well with my personal observations. Over eight years as a commercial guide in the foothills of the Sierra Nevada Mountains in California, I noticed flattening and shrinking of popular lunch and camping sand bars, especially the sand/gravel beaches used for camping on multi-day trips.

Vincent and Andrews (2008) also explored the distribution of sand beaches along whitewater rivers with a focus on their suitability for recreational use. Their study examined eight rivers in the western United States, evaluating the frequency of occurrence of useable sand bars from a recreational standpoint. Variability in size and frequency was explored in connection to flow and the prevalence of suspended sediment. Vincent and Andrews (2008) describe a decrease in the number of beaches when the flow

is regulated by a dam. They determined that a decrease in peak runoff limits the volume of entrained sediment. This, in turn, can increase the rate of erosion downstream. Therefore, beaches that typically aggrade during periods of high discharge remain unchanged or erode. Additionally, recirculation zones triggering some beach formation at high discharge levels may not experience sufficient discharge for the recirculation zone to develop and the associated beach building to occur. Such beaches may then be susceptible to increased rates of erosion during the artificially increased minimum discharges (Vincent and Andrews 2008).

Foot and Cattle Traffic

The impact of foot traffic on erosion rates is not a new topic of study (Coleman 1981; Morgan and Smith, 1980). The focus of previous work focused on recreational foot paths, and the potential for an increase in erosion rates due to increases in foot traffic (Coleman 1981; Morgan and Smith, 1980; Tomczyk and Ewentowski 2012). The quantity and type of vegetative cover, underlying geology, and slope of the path are deciding factors in predicting the rate of erosion. Coleman (1981) discusses the susceptibility of certain plant species to trampling over others. He also discusses the role of the underlying geology, noting that loosely consolidated material is more prone to erosion. In a lab experiment by Morgan and Smith (1980) the mechanics of foot strike and slope were explored in depth. They discovered that shearing forces due to the toe have the most detrimental effect on erosion rates. Slope angles of 5^{o} to 20^{o} also proved to be the most susceptible to high erosion rates. Recently, the use of Digital Elevation Model Differences (DoDs) has been employed to quantify micro changes in soil loss (Tomczyk and Ewentowski 2012). The use of DoDs proved successful in accurately

quantifying soil erosion and deposition rates at very fine scales. The above studies explored the role of human-derived trail erosion, but did not explore human-derived erosion in fluvial settings. It has been shown that repeated foot strikes have the ability to effect erosion rates, especially in unconsolidated material. The study location has slope angles that fall with the 5^{o} to 20^{o} range and are comprised almost entirely of unconsolidated material with little vegetation.

The quantification of human-induced erosion on river bar morphology has not warranted study to date. However, there is a body of work concerning the role of livestock on erosion rates of stream banks. Livestock generally use streams within their grazing area as a source of water. Repeated trips across often unconsolidated alluvium results in noticeable changes to stream morphology (Trimble 1994). The high volume of traffic these watering paths experience is similar to that seen on beaches commonly used on commercial raft runs.

The role livestock plays in the degradation of river and stream banks can be divided into either direct or indirect impacts (Evans 1998). The direct impacts on banks may be further divided between their impacts on the degradation of the bank itself, and the degradation of the vegetation covering the bank in question. Bank degradation refers to the mechanical movement of soil from the bank into the channel and its subsequent removal by the stream. The degradation of vegetation via trampling increases the erosivity of runoff. Indirect impacts concern compaction of the soils which increases the vulnerability of the bank to erosion due to additional forces such as runoff (Evans 1998). In reaches where grazing is present, livestock represent an important component in the erosion of permanent and ephemeral stream banks. Earlier studies by Kauffman and

Krueger (1984) led to similar conclusions involving the adverse effects of livestock on stream bank morphology; including the role of soil compaction and vegetation removal, resulting in an increase in the erosivity of runoff.

Trimble (1994) attempted to quantify and compare differences in erosion rates along stream banks where livestock were present versus those where livestock were not. Trimble (1994) uses the traditional method of geomorphic analysis; cross-section surveying with a surveying rod and level. He notes the limitations of his methods and that too many cross sections would be needed for the method to prove practical. Despite these challenges, Trimble observed increased erosion rates due to mechanical erosion by the livestock. He described erosion rates of three to six times greater along stream banks where livestock were present versus those where livestock were not. In Trimble's 1994 study, increased erosion rates are attributed to the mechanical breakdown of the bank associated with travel patterns of the cattle to the water. Cattle traffic mechanically loosened bank deposits which then moved into the stream channel and were eroded. In total, approximately 40 m^3 of material was removed per year over an reach approximately 400 meters long.

Research on human foot traffic shows a quantifiable impact on erosion rates. In riparian environments, cattle have been shown to have a large impact on the morphology of bars. Taking into account the number of people that use rivers in the United States for recreation during summer months and the highly susceptible nature of many of the bars to anthropogenic mechanical erosion, it is likely that river bars that experience large numbers of users will see quantifiable bar erosion due to human traffic.

Assessment of Error in Digital Photogrammetry

The most common method for assessing geomorphic change is the comparison of two digital elevation models (DEMs) from two different times. This method is referred to as a DoD, or DEM of difference (DEM differencing). The DoD method has the ability to accurately portray zones of erosion and deposition with high degrees of accuracy (Heritage et al., 2009). However, as with all remote sensing techniques, there must be an understanding of error. One of the most important current issues in the use of photogrammetry, or any optic-based DEM generating technique, is how one accounts for errors in the DEM. When using a DoD based analysis in geomorphology it is especially important to account for the uncertainty inherent in DEM generation. It is often the case that the magnitude of change anticipated is of a similar scale to the uncertainty in the DEM. If the measured change in morphology is less than the range of uncertainty associated with the DEM generation, the DoD method may treat the change as random noise within the DEM. This can lead to significant impacts on the accuracy and relevance of any findings (Wheaton et al., 2010; Milan et al., 2011). Studies using multiple styles of optically-derived DEM generation, and a DoD analysis have begun to establish techniques for accounting for uncertainty within a DEM. When considering error within the DoD method, two assertions can be made; 1) high roughness and a low point density will generate high uncertainty, and 2) low roughness with a high point density will lead to lower uncertainty.

There are three factors that play a role in the quality of a DEM (Heritage et al., 2009); 1) the quality of the data points within a surface, 2) the density of the data points within the surface, and 3) the spatial distribution of the data points within the surface. All

three are related to the method of data acquisition and processing technique. Within a point cloud, high quality (accurate) points that are densely spaced within the DEM, and evenly distributed throughout the DEM are ideal. However compromises between processing time and accuracy must be weighed. When quantifying error, Milan et al., (2011) and Heritage et al., (2009) both address a problem with DEM validation for optically-derived DEMs. In practice, when validating the precision of a DEM surface, it is compared to another, more accurate DEM. Advances in DEM resolution associated with advances in technology created a situation where more accurate DEMs do not exist. As a result, it is impossible to validate a DEM against a more accurate DEM. A number of statistical approaches are being explored in an attempt to quantify error, a description of which follows.

Wheaton et al., (2010) propose three steps that should be taken into account when considering uncertainty within the DoD model, regardless of the DEM generation method. The first step is to quantify the surface uncertainty in each DEM. Secondly, the identified uncertainty of each DEM should then propagate into the DoD using equation (1). Finally, the significance of the propagated uncertainties must is considered in the context of the specific research. This means the significant threshold for point exclusion based on a desired accuracy versus potential error in morphologic change must be weighed. In three dimensional space (X,Y,Z point cloud) the horizontal (X,Y) errors approximate those in the vertical (Z) direction. However, in low slope areas (such as depositional fluvial settings) the horizontal error has a negligible effect on distortion. As such, Wheaton et al., (2010) define the actual z deminsion within a DEM as:

$$Z_{actual} = Z_{DEM} \pm Z_{error} \quad (1)$$

Where Z_{actual} is the true location of the surface, Z_{DEM} is the location of a given point within the three dimensional point cloud and Z_{error} is the vertical error associated with DEM generation. Because it is possible to assume the vertical error is randomly distributed, and independent of the actual surface, Z_{error} can be assumed to be a single value for an entire point cloud. To then propagate the uncertainty into the DoD the following equation is used:

$$\delta_{DoD} = \sqrt{(Z_{new})^2 + (Z_{old})^2} \quad (2)$$

Where δ_{DoD} is the propagated error within the DoD and Z_{new} and Z_{old} represent the vertical error in the new (time 1) and old (time 2) DEMs being used to compile the DoD, respectively. The uncertainty range within the DoD is based on the error derived from within the DEMs being used. Greater uncertainty within the DoD means a larger threshold for exclusion of elevation data. Data exclusion stems from the idea that any change-value falling within the range of uncertainty for the DoD will be excluded. The larger the range of uncertainty, the more change-values will be excluded. This leads to an inability within the DoD to detect changes in the topography, meaning more lost topographic data and a decrease in accuracy (Wheaton et al., 2010).

A new method for deriving error developed by Wheaton et al., (2010), in response to the challenges explored above, moves beyond using a single value for uncertainty. In their new model for assessing uncertainty, a window of a predefined size moves throughout the DoD. Each cell is defined as either erosional or depositional, taking into account the surrounding cells. If the surrounding cells have one property, and the cell in question has another, it is considered an error and discarded. If the examined cell and the surrounding cells have the same property, the data will be kept, even in situations where

the data is below the uncertainty level. Separate indices (one for erosion and one for deposition) are calculated for each cell to avoid the possibility that a cell may fall in a zone of rapid transition but get discarded as uncertainty.

A similar technique was developed by Milan et al., (2011). It also involves a moving window error assessment to allow for variation in the uncertainty that may be associated with variability in the surface roughness. The chief difference is that the technique by Milan et al., (2011) uses the standard deviation of the errors between the two time-separated DEMs to propagate error into the DoD. As such, they are able to include probability, using the equation:

$$U_{crit} = t\sqrt{(\sigma_{e1})^2 + (\sigma_{e2})^2} \quad (3)$$

In this case, U_{crit} is the propagated error within the DoD; *t* is the critical *t*-value at the chosen confidence interval, and σ_{e1} and σ_{e2} are the standard deviations of elevation error. When using this method a normal distribution of errors must be assumed. A comparison by Milan et al., (2011) between raw DEM data, a single value to represent uncertainty, and a spatially distributed level of uncertainty value shows a marked difference in the level of uncertainty.

Accounting for Error When Using PhotoScan

The most common method for assessing geomorphic change is the comparison of two digital elevation models (DEMs) from two different times. This method is referred to as a DoD, or DEM of difference (DEM differencing). The DoD method has the ability to accurately portray zones of erosion and deposition with high degrees of accuracy (Heritage et al., 2009). However, as with all remote sensing techniques, there must be an understanding of error. One of the most important current issues in the use of

photogrammetry, or any optic-based DEM generating technique, is how one accounts for errors in the DEM. When using a DoD based analysis in geomorphology it is especially important to account for the uncertainty inherent in DEM generation. It is often the case that the magnitude of change anticipated is of a similar scale to the uncertainty in the DEM. If the measured change in morphology is less than the range of uncertainty associated with the DEM generation, the DoD method may treat the change as random noise within the DEM. This can lead to significant impacts on the accuracy and relevance of any findings (Wheaton et al., 2010; Milan et al., 2011). Studies using multiple styles of optically-derived DEM generation, and a DoD analysis have begun to establish techniques for accounting for uncertainty within a DEM. When considering error within the DoD method, two assertions can be made; 1) high roughness and a low point density will generate high uncertainty, and 2) low roughness with a high point density will lead to lower uncertainty.

There are three factors that play a role in the quality of a DEM (Heritage et al., 2009); 1) the quality of the data points within a surface, 2) the density of the data points within the surface, and 3) the spatial distribution of the data points within the surface. All three are related to the method of data acquisition and processing technique. Within a point cloud, high quality (accurate) points that are densely spaced within the DEM, and evenly distributed throughout the DEM are ideal. However compromises between processing time and accuracy must be weighed. When quantifying error, Milan et al., (2011) and Heritage et al., (2009) both address a problem with DEM validation for optically-derived DEMs. In practice, when validating the precision of a DEM surface, it is compared to another, more accurate DEM. Advances in DEM resolution associated

with advances in technology created a situation where more accurate DEMs do not exist. As a result, it is impossible to validate a DEM against a more accurate DEM. A number of statistical approaches are being explored in an attempt to quantify error, a description of which follows.

Wheaton et al., (2010) propose three steps that should be taken into account when considering uncertainty within the DoD model, regardless of the DEM generation method. The first step is to quantify the surface uncertainty in each DEM. Secondly, the identified uncertainty of each DEM should then propagate into the DoD using equation (1). Finally, the significance of the propagated uncertainties must is considered in the context of the specific research. This means the significant threshold for point exclusion based on a desired accuracy versus potential error in morphologic change must be weighed. In three dimensional space (X,Y,Z point cloud) the horizontal (X,Y) errors approximate those in the vertical (Z) direction. However, in low slope areas (such as depositional fluvial settings) the horizontal error has a negligible effect on distortion. As such, Wheaton et al., (2010) define the actual z deminsion within a DEM as:

$$Z_{actual} = Z_{DEM} \pm Z_{error} \quad (1)$$

Where Z_{actual} is the true location of the surface, Z_{DEM} is the location of a given point within the three dimensional point cloud and Z_{error} is the vertical error associated with DEM generation. Because it is possible to assume the vertical error is randomly distributed, and independent of the actual surface, Z_{error} can be assumed to be a single value for an entire point cloud. To then propagate the uncertainty into the DoD the following equation is used:

$$\delta_{DoD} = \sqrt{(Z_{new})^2 + (Z_{old})^2} \quad (2)$$

Where δ_{DoD} is the propagated error within the DoD and Z_{new} and Z_{old} represent the vertical error in the new (time 1) and old (time 2) DEMs being used to compile the DoD, respectively. The uncertainty range within the DoD is based on the error derived from within the DEMs being used. Greater uncertainty within the DoD means a larger threshold for exclusion of elevation data. Data exclusion stems from the idea that any change-value falling within the range of uncertainty for the DoD will be excluded. The larger the range of uncertainty, the more change-values will be excluded. This leads to an inability within the DoD to detect changes in the topography, meaning more lost topographic data and a decrease in accuracy (Wheaton et al., 2010).

A new method for deriving error developed by Wheaton et al., (2010), in response to the challenges explored above, moves beyond using a single value for uncertainty. In their new model for assessing uncertainty, a window of a predefined size moves throughout the DoD. Each cell is defined as either erosional or depositional, taking into account the surrounding cells. If the surrounding cells have one property, and the cell in question has another, it is considered an error and discarded. If the examined cell and the surrounding cells have the same property, the data will be kept, even in situations where the data is below the uncertainty level. Separate indices (one for erosion and one for deposition) are calculated for each cell to avoid the possibility that a cell may fall in a zone of rapid transition but get discarded as uncertainty.

A similar technique was developed by Milan et al., (2011). It also involves a moving window error assessment to allow for variation in the uncertainty that may be associated with variability in the surface roughness. The chief difference is that the technique by Milan et al., (2011) uses the standard deviation of the errors between the

two time-separated DEMs to propagate error into the DoD. As such, they are able to include probability, using the equation:

$$U_{crit} = t\sqrt{(\sigma_{e1})^2 + (\sigma_{e2})^2} \quad (3)$$

In this case, U_{crit} is the propagated error within the DoD; *t* is the critical *t*-value at the chosen confidence interval, and σ_{e1} and σ_{e2} are the standard deviations of elevation error. When using this method a normal distribution of errors must be assumed. A comparison by Milan et al., (2011) between raw DEM data, a single value to represent uncertainty, and a spatially distributed level of uncertainty value shows a marked difference in the level of uncertainty.

DEM Differencing Using CloudCompare

CloudCompare is an open source 3D point cloud and mesh comparison software tool. Recent updates have seen the addition of the M3C2 plugin which allows DEM differencing to be done using a different approach than previous CloudCompare versions. The M3C2 algorithm is unique in that calculations are based on a cylinder of defined diameter (*d*), where the axis goes through point *i* and the cylinder is oriented tangential to the surface at point *i* (Lague et al., 2013). This method has three predominant benefits as they relate to the present study: 1) It allows for a new layer file to be created where each point at location *XY* has a signed *z* value representing the distance between the two original DEMs, 2) one optional output is the significance of change Chi2 test for any change between the two DEMs and 3) because differences in the *z* direction between the two DEMs are calculated using a series of cylinders of known dimensions it is possible to calculate positive (deposition) and negative (erosion) volumetric change. For an in depth discussion of how the M3C2 plugin works, see Lague et al., (2013).

Objectives

The aim of this study is to contribute to the emerging body of literature on digital photogrammetry, specifically as it applies to the study of fluvial geomorphology. An effective workflow for photoset acquisition, processing, and analysis is presented using commercially available software and open source software. Two different studies are then described. Initially, I present a controlled experiment to show the practical limitations of digital photogrammetry in geomorphic settings. The experiment uses four clasts of different sizes to simulate erosion and deposition. The experiment is done on two different bars, one composed of gravel size particles and one of coarse sand. Using the same technique, the location and quantity of erosion and deposition at five river bars along a popular commercial whitewater rafting run are described. The river bars vary in size from $15m^2$ to $30m^2$. They were chosen based on their popularity as lunch stops for commercial and private river runners. The timing for photoset generation was chosen to highlight the impacts of the river users on bar morphology.

Chapter Two: Method

General Workflow

The workflow described here is for close-range digital photogrammetry (as defined by Matthews (2008)) for the commercially available software PhotoScan (© 2014), and the open source software CloudCompare (2014). I describe the process for photoset generation including what must be done in the field to establish scale and align point clouds for later analysis. I then describe an effective workflow for processing a photoset using PhotoScan which results in a sparse point cloud. I also include suggestions for thresholds when refining the sparse point cloud. After the sparse point cloud has been refined, I describe how to establish real-world scale and identify ground control points. A copy of my workflow diagram for photo processing can be seen in figure 1, below.

Figure 1

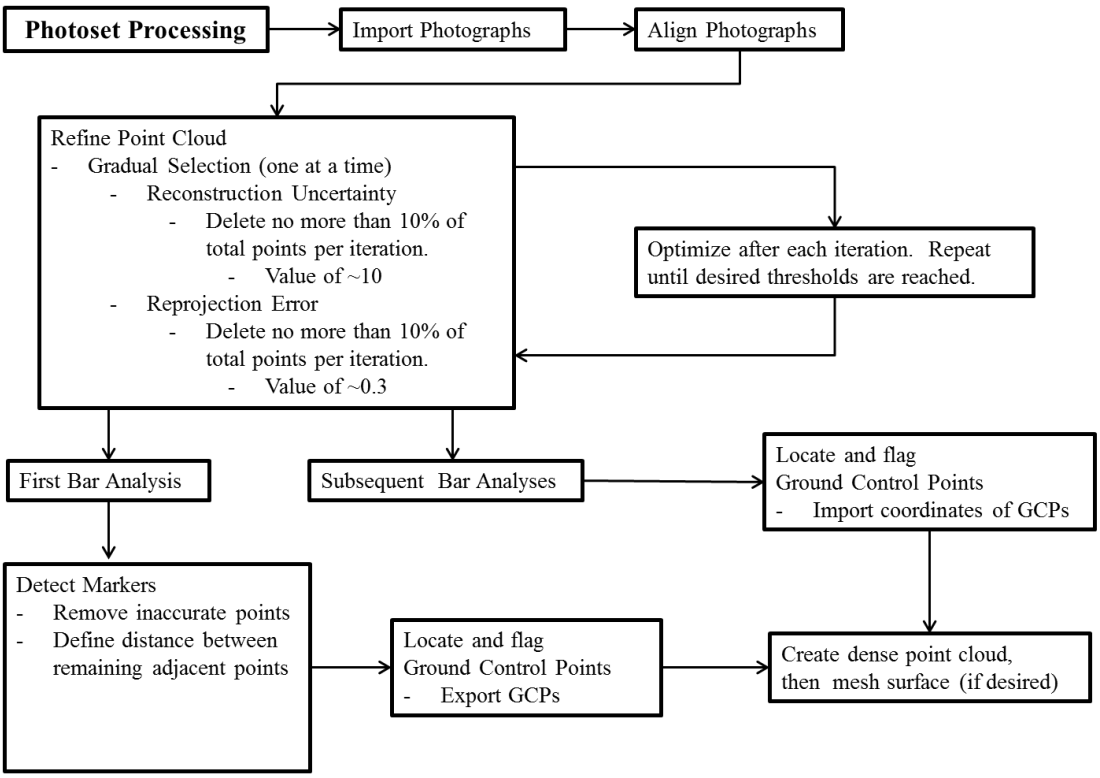

General workflow for processing a photoset using PhotoScan. Workflow developed by the author.

For all photosets I used a Nikon D5200 DSLR camera with a fixed, 28mm focal length lens. The camera was mounted on a 1.8 meter monopod to ensure a consistent object-to-camera distance. The uniquely coded scale-bars used to establish scale are available through the *tools* menu in PhotoScan and were mounted to a ridged plastic backing.

Image Acquisition

Before beginning to take pictures, the scale bars were randomly distributed throughout the landscape and ground control points (GCP) were established. Figure 2 shows the camera setup while in the field. Figures one and two in Appendix A are: of a GCP in the field and a scale bar. Ground control points are small features permanently

Figure 2

Taking pictures in the field. Camera is mounted on the monopod.

located within the landscape. The smaller they are, the more accurate subsequent digital elevation model (DEM) alignment will be. However, camera-to-object distance must be considered to ensure that the GCP are identifiable in photographs. A minimum of three GCP are needed, and they should not be placed linearly. The number and size of GCP,

and number of scale bars included in the photoset will be dictated by the size of the study area. Larger study areas will require more scale bars and larger, more abundant GCP. Once the coded scale bars and GCP are present, the photoset can be taken. If the inclusion of scale bars is not practical, it is possible to forgo their inclusion. Alternately, the distance between all GCP is measured. When creating scale, this is the distance that was used.

For successful point cloud construction, I ensured each photograph overlapped with adjacent photographs approximately 66%. The closer the camera-to-object angle is to perpendicular, the less distortion there will be and therefore the more accurate the spares point cloud. I also ensured that each scale bar and all ground control points were included in the first photoset as well, following the same principle of camera overlap. After generating the first photoset, the scale bars no longer need to be included in subsequent photosets. I included the ground control points in all photosets for DEM alignment.

Photoset Processing, Post-Processing, and Point Cloud Refinement

The first step in processing is to bring the photoset into PhotoScan, using the *Workflow* menu. Once the entire photoset has been uploaded, I began the photo-alignment process. Initial photo alignment often took take several hours, depending on the number of pictures within the photoset and the area covered by each photograph. The result was a sparse point cloud.

Within the PhotoScan software there are two tools to minimize pixel location uncertainty and resulting error; *reconstruction uncertainty* and *reprojection error*. I used

both tools after the initial photo alignment that resulted in the sparse point cloud. Both tools work by removing pixels that have been aligned within the sparse point cloud, but have a higher magnitude of uncertainty in their location than desired. They both allow an ideal threshold for accuracy to be reached after the initial aligning phase of sparse point cloud reconstruction. With each iteration, a certain number of points (matched pixels) were selected by the software. These are the points with the largest uncertainty in their location. I then deleted them and re-optimized the sparse point cloud based on the remaining points. The accuracy of the software to match pixels between stereoscopic images increases with each optimization, therefore decreases the number of mismatched or misplaced pixels and the associated error. I used the reconstruction uncertainty to remove points whose locations show large deviations from the point cloud surface; noise in the Z direction within the point cloud. I used the reprojection error tool to address the spatial location of matched pixels within the point cloud. While the ideal error threshold is different, point deletion and optimization are carried out in the same manner. Reprojection error refines the spatial location and alignment of the points. Decreasing the reprojection error correlates directly with increasing the accuracy of the digital surface. The optimization of photo alignment refines the algorithm, increasing the accuracy of point placement I used multiple iterations of the reconstruction uncertainty and reprojection error tools increase the ability of the software to spatially place pixel matches. For example, upon initial photo alignment, a number of photogrammetrically matched points may have a spatial error of ±10 pixels. They will all get removed because the uncertainty of their location is higher than desired. Optimization after each point

deletion, at each iteration leads to more accurate pixel matches, less uncertainty in point locations, and therefore lower error. Based on a series of conversations with T. Noble, photogrammetrist at the USGS, and personal experimentation, I found a reconstruction uncertainty value of approximately 10 and a reprojection error value of approximately 0.3 were ideal. These values preserved the detail of the sparse point cloud while maintaining the accuracy needed for detecting fine scale change (personal communication, 2014). Additional refining jeopardizes the software's ability to generate the dense point cloud and does not yield more accurate results. Having refined the algorithm by which PhotoScan aligns pixels, dense point cloud generation within this project becomes more accurate. I repeated the process of photo alignment and point placement refinement is repeated for every river bar at every time step.

Scale Establishment

After the sparse point cloud has been refined, I established real-world scale and identify ground control points. The software can recognize and flag the center points of the coded scale bars. This inevitably resulted in the identification of extraneous points, which I deleted. I made sure to examine individual pictures containing a flag and adjust the location of the flags to ensure that they were, in fact, centered within a coded target. This helped improve the accuracy of the scale. To establish the real-world scale, I flagged two markers (either on a scale bar or two GCP) and defined the distance between them.

I established ground control points from individual photographs within the project. I opened a photograph that included one or more GCPs and flagged (and named) it. After flagging the same GCP in two photographs, the software will recognize its

location within the sparse point cloud, and place a flag on the GCP in every other photograph it appears in. It is still necessary to refine the location of the flag in each photograph as I did with the scale bars. I repeated this step for each GCP. Once all of the GCPs were flagged, I optimized the project once more, thus calculating the actual error in real-world dimensions. Using the software, I extrapolated the location of the GCP in terms of real-world scale as designated by the scale bars. The final step I used for GCP establishment was to export and save the GCP coordinates. In subsequent DEMs of the same study area, I imported the GCP coordinates for that beach, establishing the same real-world scale and placing the two bars in identical three dimensional space.

The final step before any analytics can be done occurs after refinement of the sparse point cloud and establishment of ground control points and scale. First, I made a dense point cloud using the PhotoScan workflow, and based on the dense point cloud, a mesh surface. When exporting the mesh surface, I made sure that the bounding box and point spacing were consistent for each beach at each time.

Analysis Using CloudCompare

All statistical analysis for this study was done using the open source software CloudCompare and the plugin M3C2. The M3C2 tool calculates distances between two digital elevation models (DEMs) using a cylinder to integrate change between the two, where cylinder area is defined by the user based on surface roughness, detail desired and processing time and height is based on a maximum anticipated change. See Lague et al (2013) for a detailed description of M3C2.

For this study, for all locations at all times, I exported the mesh surfaces from PhotoScan using a point spacing of 0.01 meters. This was chosen to ensure sufficient detail of the surface to capture the complex nature of the beaches being studied and the fine-scale change I anticipated. I defined my cylinder diameter as 0.01 meters as well so that there would be a change estimation associated with each data point and data loss due to averaging would be minimal. Cylinder height was set at between 0.5 and 2.0 meters, depending on location and the magnitude of change anticipated.

The output I used in this study was gradient distance which returns a signed distance value between the two DEMs in the z direction. I calculated volume of change based on the gradient distance output layer and the local statistics for that layer. To calculate volume of change, I created two new layer files; one where $z \geq 0$ and one where $z \leq 0$. These two new layer files can then be exported to excel where raw values are visible; specifically, the total number of valid points and the sum of all values in the z direction, ($\sum z_i$). Having defined the radius of the cylinders earlier, I calculated the volume of morphologic change as (equation 4):

$$V = \#\ valid\ points \times (\pi r^2) \times (\sum z_1 z_2 z_3 \dots z_i) \quad (4)$$

Independently for all +z values (deposition) and all -z values (erosion). I used the above described workflow for all DEM generation, DoD analysis and volume calculations.

2.6. Particle Size Distribution

The distribution of particle size for each beach was done using six samples from two transects from each bar, 24 samples in total. The samples were taken on 7/29/2014 (t8). Transects moved from the water inland, and were located to cross the zones of

largest change and/or heaviest use. Three samples were taken along each transect, consisting of a depth of approximately 5cm.

I conducted the particle size analysis in the soil laboratory at the University of Denver Geography Department using a series of soil sieves. I took a wet weight of each sample, dried the samples, and then reweighed each dried sample. Each dry sample was then passed through the sieves stacked in descending order of sizes (in mm): 5.60, 4.00, 2.80, 2.00, 1.00, 0.50, 0.15. The captured sediment was then weighed separately, allowing for the calculation of a percent of the total sample. Tables of the wet and dry weights, as well as the weights of each clast size can be seen in Appendix A, table.

Chapter Three: Practical Experiment

Experimental Design

In order to assess the practical limits for change detection using PhotoScan and CloudCompare, I developed a straight forward experiment. I generated two photosets, at two different locations, of approximately 40 pictures each using the same camera and monopod set up described at the beginning of section 2 and seen in figure 2 (above). The locations were a gravel bed with a mean particle size of approximately 2.0 cm (L1) and a sand bar comprised of predominately coarse sand (L2). At each location, I took two photosets, one as time zero (t0) and one as time one (t1). For the simulation I selected four approximately spherical clasts of known size: circumference = 2.0 cm, 9.0 cm, 16.5 cm and 28 cm, respectively. After the first photoset (t0) I moved the four clasts, simulating erosion; and placed them in a different location, simulating deposition. I then took another photoset (t1).

The photo processing was done using PhotoScan based on the uncertainty tolerances described in section 2.2. I generated a sparse point cloud, and from the refined sparse point cloud, I generated a dense point cloud and finally a mesh surface. For times t0 and t1, I exported the mesh surface with a point spacing of every 0.005 meters. The point cloud assessment was done using the M3C2 tool within the software CloudCompare. The result was two DEM point clouds where each point has a corresponding point in the other cloud. Designating t0 as the referenced cloud, any

change in point location result in a signed distance in the z direction, known as the gradient distance. Knowing the size of the four clasts allowed me to create DoDs where the location and quantities of erosion and deposition were known. I was therefore able to compare the volume of change determined by my analysis with the known volume of all four clasts.

Results and Discussion

The combined volume of all four clasts is 456cm^3. At the gravel location (L1), CloudCompare computed a total volume of deposition of 425cm^3 and the volume of erosion as 408cm^3. This represents a margin of error of 6% for deposition and 11% for erosion. At the coarse sand location (L2), CloudCompare computed a total volume of deposition of 435cm^3 and the volume of erosion as 411cm^3, representing a margin of error of 4% for deposition and 9% for erosion. As with all 3D analysis, there is some noise when using CloudCompare. In the case of CloudCompare, much of that noise is a result of imperfect alignment of the two DEMs. I accounted for that error using statistical parameters that are part of the DoD analysis. For the gradient distance, a histogram of the signed distances is created, including a mean (μ) and standard deviation (σ) where for both locations, $\mu \approx -0.0009$ and $\theta \approx 0.005$. Based on the distribution of gradient distances in the histogram, I decided that anything within ±σ was error in the model. Therefore, when calculating the volume of change I used the thresholds $z \geq \sigma$ and $z \leq \sigma$. This decision was justified by the accuracy with which the model was able to calculate the known change. Having shown the effectiveness of the method, I then moved to a field application.

Chapter Four: Field Application

Location: Browns Canyon, Arkansas River, Colorado

The Upper Arkansas Basin is in the northern part of the Rio Grande Rift, It formed as a down-faulted trough (DeWitt & O'Neill 1998) approximately 29 million years ago (Tweto 1979) and covers 3155 km^2 (DeWitt & O'Neill 1998). The floor of the valley is a result of this glacial outwash and is known as the Dry Union Formation. The Dry Union Formation is comprised of silts, sand and gravel from alluvial fans created by glacial melting. Glacial erosion as well as the work of rivers and streams has done much to create the more gentle terrain on the valley floor we see today (Tweto 1961). The most recent glacial advance also pushed the Arkansas River to the western side of the valley where it has incised through the Dry Union formation to the hard, Precambrian Granodiorite (Karnuta, 1995). This Precambrian Granodiorite comprises much of the channel through Browns Canyon.

The water in the Arkansas River is a combination of seasonal snow melt, and flow augmentation from a number of transmountain diversions and reservoirs. During peak run off, usually June or early July, water diversion and storage rates increase. Water is diverted from other drainage basins and stored in Twin Lakes Reservoir and Turquoise Reservoir (DeWitt & O'Neill, 1998). The schedule for release, and vlume of water released are adjusted yearly based on the snowfall totals for the Arkansas drainage basin and surrounding contributing basins. Additional changes to releases from the

contributing reservoirs are made hourly based on changing snowpack melt rates due to atmospheric conditions such as rainfall. A hydrograph of the average daily discharge for calendar years 1964 to 2013, the study period, study days and rainfall are shown in figure 3, below.

Figure 3

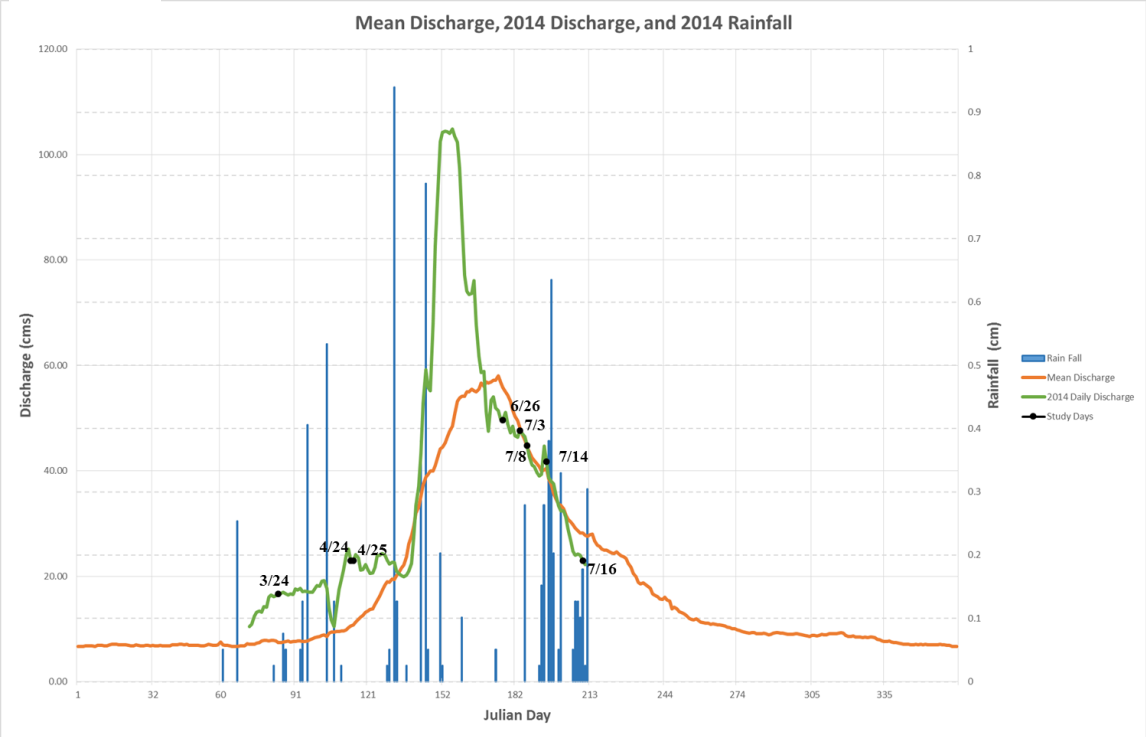

Average annual discharge for Brown's Canyon and daily rainfall totals. Mean discharge computed from the mean daily discharge for each day from 1964 to 2013 record. 2014 average discharge computed from daily average discharge. The data are from USGS gauge 07091200, near Nathrop, Colorado (accessed 5/10/2014 and 7/31/2014). Peak discharge historically occurs on June 24th, Julian day 175. Study days are indicated by a black dot.

The specific study area is the Browns Canyon section of the Arkansas River, near Buena Vista, central Colorado. The stretch of river being studied runs south, along the eastern edge of a graben known as the Rio Grande Rift. The greater watershed is known as the Arkansas Headwaters Recreation Area (AHRA) and is managed by Colorado Parks and Wildlife. Browns Canyon is approximately centered within the recreation area. In

2012, the AHRA reported 78,044 commercial rafting clients and a total of 95,547 commercial river users, including commercial guides and kayakers that ran Browns Canyon. During the 2013 season, the total number of commercial rafting clients was 86,380, and the number of commercial river users was more than 120,000 (see table 1). The Browns Canyon section of the Arkansas River is approximately 11.25 kilometers in length and has an average gradient of 1.5%. Three of the four river bars were chosen for this study because of their sandy composition and frequent use by commercial and

Table 1

2012 Season

	Rafts	Kayaks	Clients	Staff
Month				
April	27	6	96	34
May	1295	50	5601	1326
June	4706	307	22988	4802
July	6754	555	34629	6898
August	2875	361	14135	2992
September	120	31	571	132
October	3	3	24	6
totals	15780	1313	78044	16190
total users	95547			

2013 Season

	Rafts	Kayaks	Clients	Staff
Month				
April	4	14	32	10
May	1125	94	4979	1171
June	4477	186	23118	4538
July	7401	377	40230	7513
August	3419	301	17330	3534
September	155	53	661	174
October	2	3	30	7
totals	16583	1028	86380	16947
total users	120938			

Monthly Average

April	4
May	252
June	1085
July	1683
August	725
September	31
October	1

Commercial river user numbers for the 2012 and 2013 season broken down by month. Data are from Arkansas Headwaters Recreation Area yearly use report. (Unpublished as of 5/1014. Data acquired via personal request.)

private river runners as a lunch stop. The fourth bar was chosen because of its similar shape and composition but infrequent use. All four beaches are sorted vertically with gravel sized clasts beginning to appear between one and three centimeters below the surface. The predominant sediment makeup of the surface of each beach is sands of a phi (φ) scale size of 1 to 2 with some gravels as well (φ -3 to -5). Beach #2 and #3 had 10 to 40 percent more fine particles (less than φ 2) than beaches #1 and #4, depending on the location of the sample. All of the beaches are between $10m^2$ and $30m^2$. A map of the study area can be seen in figure 4.

Figure 4

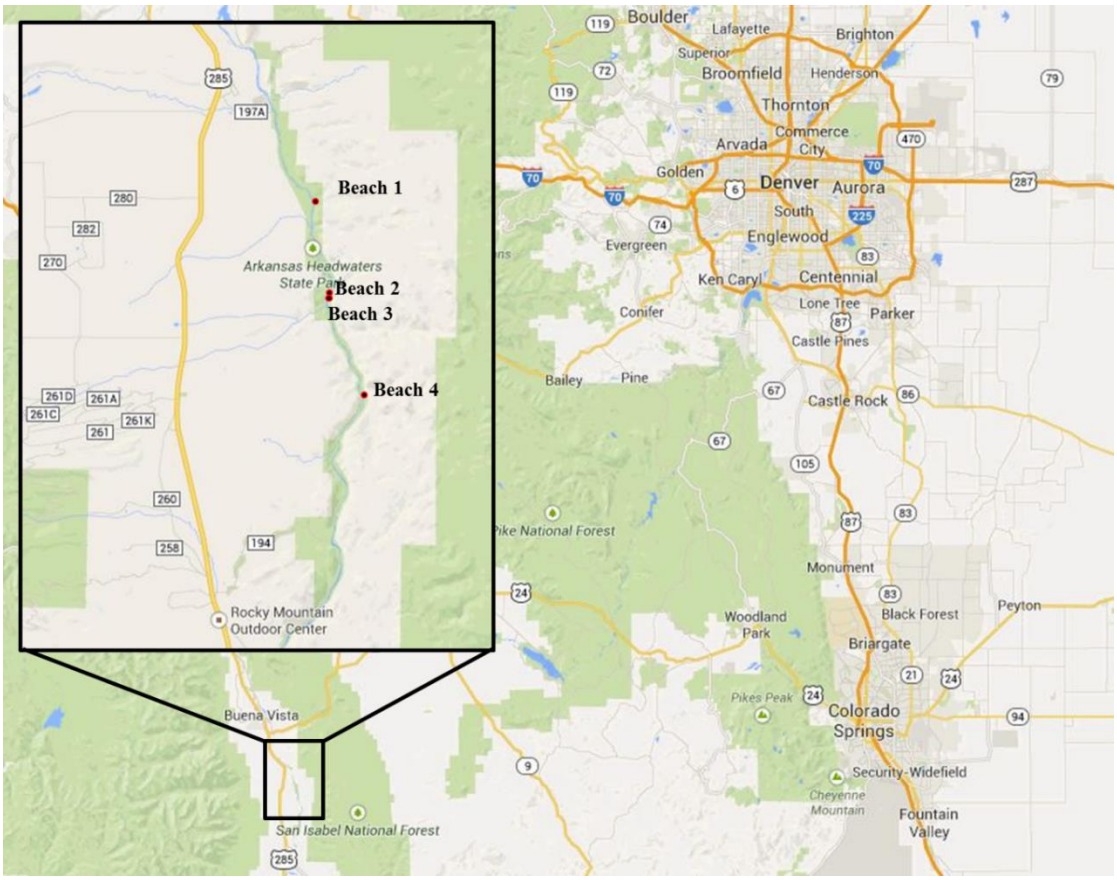

The study locations are numbered from one to four, with beach one the furthest upstream and subsequently numbering based on downstream travel (see inset, figure 4). Its proximity to the beginning of the put in for commercial rafting trips, and clast size distribution representative of the other three river bars make it is an appropriate bench mark when trying to separate fluvial change from anthropogenic. Beaches two and three contain standard BLM camping signage regarding acceptable use and required equipment for camping. They are popular for lunch stops as well as overnight camps. Beach four is directly above one of the largest rapids on the stretch of river known as Zoom Flume. It is commonly used to scout the rapid before running it. Pictures of each bar in the study can be seen in Appendix A, figure 7. A point cloud representation of each bar including

location of ground control points and approximate location of sediment sample locations can be seen in Appendix A, figures 3 through 6.

Results

All four bars in the study area were photographed between six and eight times and data was processed using the workflow outlined in section two and figure 1. Daily minimum, maximum and average discharge for each study day can be seen in table 2. On field days, photosets were taken beginning at 07:00 to be on the water before commercial rafters or after 16:00 to be on the water after commercial rafters. Despite this timing, there were occasions where beaches two and three were occupied by commercial or private boaters and photosets couldn't be taken. For all four river bars, the majority of

Table 2

Date	3/24/2014	4/24/2014	4/25/2014	6/26/2014	7/3/2014	7/8/2014	7/14/2014	7/16/2014
Minimum Q	15.82	20.64	21.34	47.92	46.48	37.24	39.76	21.17
Maximum Q	16.74	25.03	25.03	51.31	49.56	42.84	53.20	24.08
Average Q	16.34	22.97	22.93	49.62	47.57	41.10	41.73	22.94

Minimum, Maximum and Average discharge for all study days. Discharge is measured in cubic meters per second. The data are from USGS gauge 07091200, near Nathrop, Colorado (accessed 5/10/2014 and 7/31/2014)

morphologic change occurred during spring runoff, with bars one and four experiencingparticularly large quantities of deposition. River bars two and three saw some morphologic change as well over the duration of the summer, although deposition and erosion volumes were less and not as spatially clustered. Table 3 shows the volume of change for each bar from each DoD. Raw data from all river bars was processed using the workflow outlined in section two, and mesh surfaces were exported with a spacing of one point every 0.01 meters. Time t1 was used to generate the ground control points. However, spatial gaps in the DEM due to field inexperience render the DEMs themselves

ineffective for use in DoD analysis. Therefore, the earliest DEM for all analysis is time t2. These gaps did not impact my ability to develop sufficiently accurate ground control points.

Between times t3 and t4, discharge through the study area peaked at 104.8 cubic meters per second. Ground control points were covered at all beaches except beach #3 until time t5. The time-step t3-t5, or t3-t4 for beach #3, represents the period of time

Table 3

Beach #1

	Deposition	Erosion
t2-t3	0.17	-0.26
t3-t5	34.58	-6.51
t5-t6	1.11	-2.35
t2-t7	0.09	0.00
t7-t8	0.00	-7.08

Beach #2

	Deposition	Erosion
t2-t3	0.52	-0.24
t3-t5	3.09	-1.61
t5-t6	0.18	-0.32
t2-t6	4.69	-1.25

Beach #3

	Deposition	Erosion
t2-t3	1.65	-1.45
t3-t4	2.45	-4.48
t4-t7	6.72	-0.50
t2-t7	1.43	-0.82

Beach #4

	Deposition	Erosion
t2-t3	0.04	-0.98
t3-t5	86.62	-0.46
t5-t6	2.59	-0.65
t6-t7	0.06	-10.28
t7-t8	0.18	-20.63
t2-t8	62.44	-1.23

Cubic meters of deposition and erosion for each beach at each time-step.

when all beach change that occurs is due to fluvial processes. This time period is when the majority of morphologic change occurred, generally as deposition. On the rising limb of the hydrograph (times: t2 and t3) erosion and deposition levels tended to be small and similar. Additionally, times t2 to t3 encompass a 24 hour period with approximately four river users and no rainfall. The DEM of difference (DoD) encompassing peak runoff shows deposition on the order of cubic meters to tens of cubic meters for all beaches

except beach #3 which experienced erosion. On the falling limb of the hydrograph, the general trend for all beaches was either stability or erosion. The DoD analysis only included areas of DEM overlap. Thus, volume of morphologic change could not be influenced by an increase or decrease in the total area of bar exposed related to changes in discharge. The DoDs for all beaches at all time-steps are as follows: Beach #1, Appendix B; Beach #2, Appendix C; Beach #3, Appendix D; Beach #4, Appendix E.

Expanding on suggestions from Wheaton et al. (2009), I use the average volume of deposition and erosion for this 24 hour period to represent the uncertainty in the actual volume of morphologic change. As such, I report all change values as +/- the deposition or erosion value calculated between times t2 and t3. By doing this, I make the assumption that between times t2 and t3 there was no detectable morphologic change. Therefore, any change shown has occurred in error. I chose to use the time t2 to t3 values for each beach separately to acknowledge that each beach will likely have different uncertainty values based largely on my ability to consistently locate ground control points in the photographs.

Figure 5

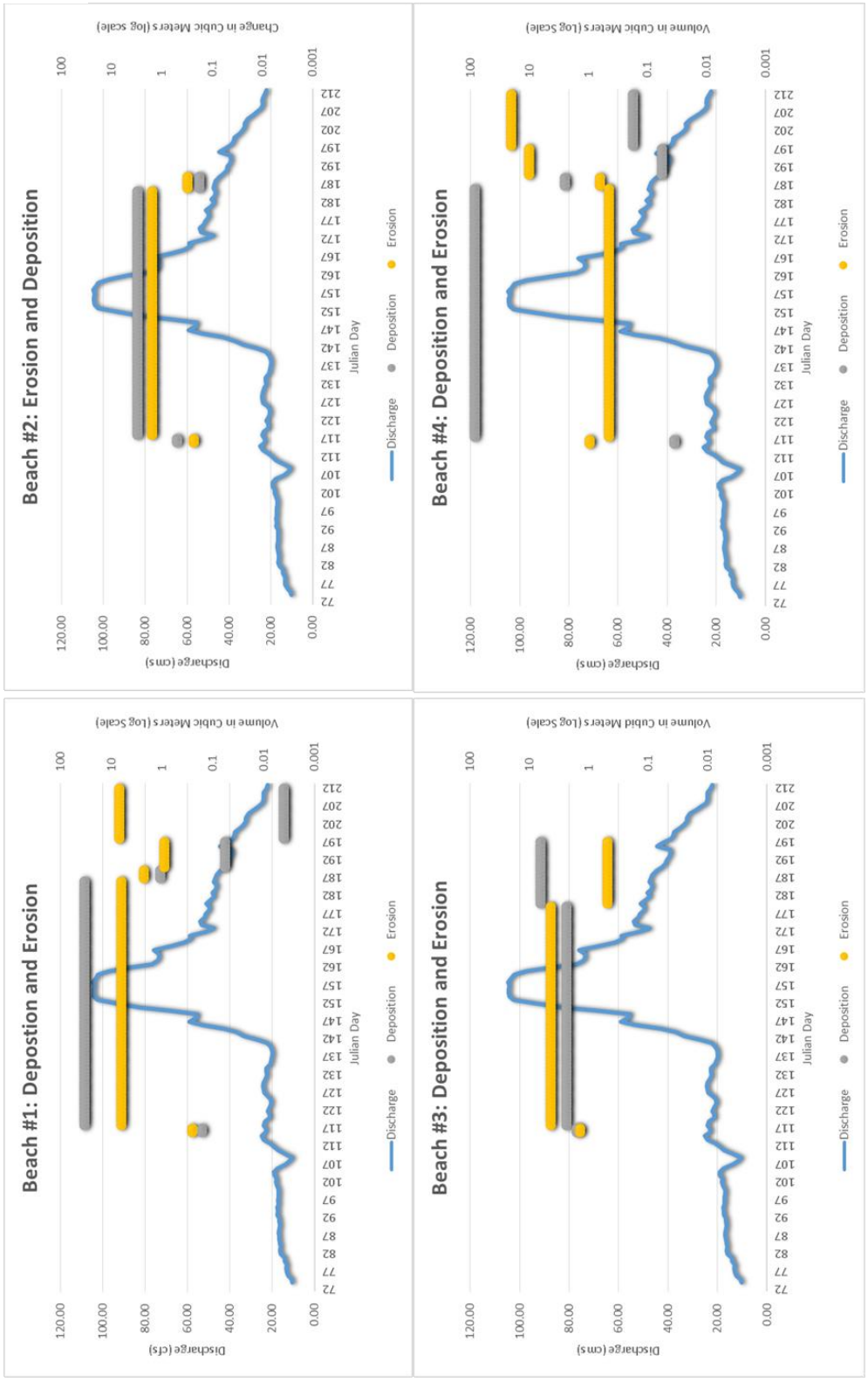

Deposition and Erosion values for each beach. Discharge through the season is shown in blue. The extent of the deposition and erosion bars indicates the time between each DEM generation.

Beach #1

On the rising limb, beach #1 saw virtually no change during the 24 hours between times t2 and t3. The error associated with deposition is +/- 0.17m^3 and for erosion it is +/- 0.26m^3. The largest morphologic change occurred during peak runoff, with deposition of approximately 34.5m^3, located almost entirely at the north side of the bar, which filled in an old channel from a wash. As discharge fell, the volume of change remained minimal with erosion and deposition volumes remaining approximately even. This was seen in the DoD analysis from times t5 to t6 and t6 to t7 (see table 3). At the end of the study period, between times t7 and t8, there were a number of rain storms in the area, one of which resulted in the reestablishment of the wash channel at the north end of the beach. The channel creation resulted in the erosion of approximately 7m^3 of material. For the duration of the study, time t2 to t8, the volume of material at beach #1 remained general constant. Cross sections of the DoD from time t3 to t5 and t7 to t8 can be seen in Appendix B, figure 1. Figure 6, above, shows the deposition and erosion values for all DoDs for beach #1.

Beach #2

Beach #2 was less frequently photographed due to the presence of commercial river users. The patter, of little change, deposition, and little change during the rising limb, peak discharge, and falling limb respectively, was similar to that of beach #1. During the early portion of the season, there was little morphologic change, with deposition and erosion values being approximately equal. The error associated with

deposition is +/- 0.52m^3 and for erosion it is +/- 0.24m^3. During peak runoff, there was deposition of approximately 3m^3 of sediment. Bar use increased considerably during the falling limb and the only DoD that was possible give the data was times t5 to t6. This DoD does not show particularly large volumes of deposition or erosion. Deposition and erosion totals can be seen in table 3. Over the duration of the study (times t2 to t6 for this bar), the general trend appears to be one of deposition. The implications of which are discussed further in the discussion, section 5.1.2. The deposition and erosion values for all of the DoDs for beach #2 can be seen in Figure 5.

Beach #3

Beach #3 saw a different morphologic trend during peak runoff than that of beaches #1, #2 and #4. The error associated with deposition is +/- 01.65m^3 and for erosion it is +/- 1.45m^3. During peak runoff (captured by DoD times t3 to t4), the predominant morphologic change was that of erosion, approximately 4.5m^3, however there was some deposition as well of approximately 2.5m^3 (see table 3). The DoD analysis capturing the falling limb of the hydrograph (times t4 to t7) shows deposition of approximately the same volume as the erosion associated with peak runoff. During the 24 hour period between times t2 to t3, erosion and deposition values were approximately the same. Additionally, for the duration of the study (times t2 to t7) the total beach volume stayed approximately the same, with deposition and erosion values being approximately the same. Potential explanations for the deposition that occurred between times t4 to t7 are discussed in section 5.1.3. Deposition and erosion values for all DoDs for beach #3 can be seen in Figure 5.

Beach #4

Beach #4 saw the most morphologic change during the study period, both as deposition and as erosion. During the rising limb of the hydrograph, this change was consistent with beaches #1 and #2 with little morphologic change occurring during the 24 hour period between times t2 and t3. The error associated with deposition is +/- 0.04m^3 and for erosion it is +/- 0.98m^3. During peak runoff (captured by the DoD between times t3 and t5) a considerable quantity of deposition occurred, approximately 86m^3 (table 3). Unlike the other three beaches, during the falling limb all of the DoDs reveal consistent erosion of tens of cubic meters. The DoD for times t6 to t7 and t7 to t8 show a combined erosion of almost 31m^3 of sediment. Despite the volume of erosion during the falling limb, the trend of the study time period (times t2 to t8) was one of deposition, approximately 62m^3 in total. A cross section of the analysis showing the erosion that occurred between times t6 to t8 can be seen in Appendix E, figure 1. The deposition and erosion totals for each DoD can be seen in Figure 5.

Chapter Five: Discussion

General Morphologic Change

The results from this study offer three conclusions with respect to the study objective to determine what impacts river users may have on bar morphology as set up by the hypotheses. They are 1) there was a quantifiable change in river bar morphology, 2) that it is possible to draw a correlation between morphologic change and the number of river users on some of the river bars in the study, and 3) that the change that may be attributed to recreational river users is less than the change due to peak runoff for the study period, March through July 2014. This conclusion is based on measurable bar change that can be attributed to direct human impacts during the study period. Differentiation between fluvial and human impacts was most readily done by comparing the nature of beach morphology during the falling limb to average daily river users and to the DoD encompassing peak discharge.

The impact of recreational river users was most apparent and easiest to identify at beach #4. The overall lack of morphologic change and relatively few recreational river users at beach #1 helps support this claim. The impact of human use on bar morphology can be separated from other potential sources of morphologic change using the timing of DoDs as well as examining other potential sources of morphologic change such as rain events. During the early season, commercial river users average approximately four per day (table 1). The DoD for the 24 hour period between time t2 and t3 reveals very little

morphologic change with virtually no river users, no change in discharge and no rain events. Because the primary factors influencing bar morphology were constant, I consider this period of time a baseline for a lack of change. During the period between times t3 to t5, the beaches in the study area were underwater, meaning human impact wasn't possible and rainfall could not impact shape. However, the DoDs from this time period reveal a general trend of deposition, the cause of which therefore must be fluvial. During the falling limb, unused river bars would be expected to undergo little morphologic change, similar to what all beaches saw between times t2 to t3. Because discharge is falling, erosivity of the water is decreasing and erosion would be minimal. Rainfall events may trigger erosion (as seen at beach #1). However, given the timing of the DEMs of the frequently used river bars, and the available rainfall data it is possible to rule out this option in most situations. Therefore, it is possible to attribute the erosion that does occur human users.

Beach #1

Early photosets and field observations of beach #1 showed the remnants of a channel at the north end of the beach derived from a wash. During spring runoff, this wash was filled with sediment as seen in the DoD transect in Appendix B, figure 1. A likely reason for the deposition of sediment in this area is flow separation caused by large woody vegetation bounding the beach at the north end. For the duration of the study time, this beach remained virtually unchanged, the anticipated morphologic response for the bar that saw the fewest river users. However, between study times t7 and t8, the study area received heavy localized spring, the intensity of which can only be estimated

based on rainfall totals from the nearest gauge in Buena Vista, Colorado (see "rainfall totals" figure 3. During one of these events, another wash developed as evidenced by the channel which developed between times t7 and t8. Appendix B figure 2 for a cross section of the erosion. This small flood event removed approximately $7m^3$ of sediment that was deposited during the high spring runoff. While not human derived, this erosion event does represent an interesting source of sediment to the study area. Morphologic change during the falling limb due to human use occurred to some extent at the rest of the study beaches but is not seen at beach #1. Given the obvious impact of rain storms, it is possible to attribute the lack of morphologic change at beach #1 to the lack of human users.

Beach #2

Beach #2 exhibited the characteristic deposition between times t3 and t5. Additionally, the DoD encompassing the rising limb also showed little morphologic change as expected, considering the short time period and number of river users. The falling limb also does not reveal very much change in bar morphology. Erosion totals are larger than deposition, but not by a lot. This is perhaps attributable to the fact that there was not very much initial deposition. The implication is that due to the lack of deposition, the surface material was more consolidated than that of other beaches in the study area. The result being that the beach material was already in a relatively stable position from the perspective of erosion due to foot traffic. However, the general trend for the beach for the duration of the study period was one of deposition. Looking at the DoD (Appendix C, figure 2), the area of deposition is generally consolidated on the south

side of the beach. Field observations reveal that the river users tend use the north side of the beach, where there was no deposition. This also supports the theory that preexisting stability of the sediment played a role in the lack of erosion due to human traffic.

Beach #3

As with all four beaches, morphologic change revealed between times t2 and t3 is virtually equivalent, albeit larger than at any of the other study areas. Spatially, the random distribution of erosion and deposition suggest that part of the anomalously large volumes may be attributed to error in the DoD (Figure 2, Appendix D). This is accounted for given the larger error bars associated with beach #3. During peak runoff, beach #3 does not experience the characteristic deposition that the other beaches do. Instead, the predominant trend between times t3 and t4 is one of erosion, although there is some deposition as well. The erosion seen at beach #3 is likely due to its location in a wider, straight reach of river. While the other three beaches saw some protection from the increased erosivity of peak runoff due to meander bends or woody debris, beach #3 does not have any of these features. As a result, the above average discharge likely resulted in stronger currents across the beach and therefore erosion. The areas where deposition does occur are located downstream of the small woody vegetation that does exist. During the falling limb (DoD times t4 to t7) the beach unexpectedly saw about $6m^3$ of deposition rather than the predicted erosion. Spatially, this deposition is located over much of the study area (see Appendix D, figure3), with some erosion showing along the inland margin of the study area. There were some recorded rainfall events during the time period being examined here (see figure 3) and it is possible that surface flow from rain

events and foot traffic caused this deposition of material up-slope and outside of the study area. However, evidence for this is not conclusive. Given the results, for beach #3, it is not possible to conclusively attribute the morphologic change to either human or natural factors.

Beach #4

Beach #4 experienced the largest volume of deposition and erosion of all four beaches during peak runoff and the same small change volumes seen at the other beaches between times t2 and t3. The reason for the quantity of deposition that occurred at beach #4 is likely related to its position relative to the main channel. Beach #4 is located on the inside of an abrupt left bend in the river caused by an exposed bedrock cliff on the right, resulting in a point bar. During peak runoff when the bar was covered with water, woody vegetation along the upper edge of the point bar would contribute further to the decrease in flow velocity and therefore transport capacity. With the above average runoff during the spring of this year, beach #4 spent much of the year underwater, but with the velocity being slow enough to deposit about $86m^3$ of sediment between times t3 and t5 (see Appendix E, figure 2). During the falling limb of the hydrograph the beach #4 became rapidly exposed, leaving a near vertical interface between the water and bar.

Beach #4 is the only beach that experienced erosion that can be convincingly attributed to human foot traffic. The DoDs from the time steps that capture the falling limb of the hydrograph reveal a consistent trend of erosion. Spatially, this erosion occurs at the steep water – bar interface left by dropping discharge. The areas with the most concentrated erosion also remain in the same area as discharge drops (Appendix E,

figures 5 and 6). The timing of this erosion is also consistent with the largest number of average daily river users, with approximately 1,680 people using the river every day. Figure 2 in Appendix E is the transect of the DEMs used for the times t6 to t8. They show the same general flattening of the bar I noticed during my time as a raft guide in California. It is possible to eliminate rainfall as making a meaningful contribution to the trend of erosion due to the location of railroad tracks which provides a barrier between the hill slope and beach #4. The effect of the railroad tracks is that runoff from the hill slope adjacent to the beach would be blocked and therefore could not impact the study area.

Use patterns for beach #4 mimic that of cattle moving between the water and the shore. River users commonly get out at beach #4 to look at the rapid downstream before running it. Frequent travel between boats and shore fits the description Evans (1998) gives of direct impacts on beach degradation. In his definition, this kind of travel is responsible for the physical movement of bank material down slope. Related to this is the work done by Quinn et al., (1998) on the susceptibility of a slope to foot traffic (or cattle in the case of Evans (1998)) based on its composition and the slope angle. Quinn et al., (1998) points out that steep banks of unconsolidated material are most prone to erosion by foot traffic.

Further examination of the erosion and deposition data for all of the beaches also reveals that in places where deposition occurs during peak run off, erosion is more likely to occur. At locations where there is little deposition such as the north side of beach #2 and beach #3 more generally, there is not very much erosion, despite a large number of

river users. A potential implication of this observation is that the rates of erosion seen at beach #4 only occurred because of the quantity of deposition. It is also likely that as the 2014 commercial rafting season progressed, the quantity of erosion seen would decrease between two later time-steps as the beach material began to achieve its angle of repose with respect to human traffic. Had the study period been characterized by average or below average peak runoff, it is likely that beach #4 would have seen deposition and erosion trends closer to those at beaches #2 and #3.

Recreation and River Bar Morphology

Initial motivation for this study is rooted in personal experience as a raft guide in California and by work by Kaplinski et al., (2003) and Vincent & Andrews (2008). The study by Kaplinski et al., (2003) on the Grand Canyon of the Colorado River describes "considerable erosion as the season progressed". The results of this study do not present the impacts of river users as statistically significant and therefore can't be described as "considerable". However, Kaplinski et al., (2003) also did not use quantitative methods which could reveal that the considerable erosion they describe was not statistically significant, as I found in Browns Canyon. Another factor that likely contributed to the discrepancies between this study and theirs is the large difference in the character of the two rivers being studied. The predominate differences being the much higher average discharge of the Colorado River and large suspended sediment load. The presence of sediment trapping dams also plays a role in increased erosion rates downstream, which may have led to the erosion of sand bars Kaplinski et al., (2003) (Petts, 1984).

This study also has potential implications for recreational river management. Specifically, I have shown that there is an impact of recreational river users on the Browns Canyon section of the Arkansas River. However, erosion due to river users is generally far less than deposition as a result of the peak runoff. Managing agencies of rivers that are sand dominated may find it worthwhile to study the impacts that river users have on their bars due to the more erodible nature of the bar material.

Structure-from-Motion and Processing Software

Over approximately the last decade, the body of work using Structure from Motion (SfM) as a technique to study bar morphology has increased and the technique has begun to emerge as a viable option in fluvial geomorphology, especially when studying settings that experience rapid change (Chandler et al., 2002; Lague et al., 2013; Marcus & Fonstad 2010; Westoby et al., 2012). My study adds to this growing body of work while expanding on the potential for use of digital photogrammetry when studying small scale change, as described by Matthews (2008) and Tomczyk & Ewentowski (2012). Digital photogrammetry and LiDAR are both capable of producing fine scale DEMs which can then be used to describe small scale change as in section 3. However, the equipment needed for digital photogrammetry is far more compact than LiDAR; I was able to do all of my field work using only my kayak. The relatively compact size and lower costs associated with the equipment make digital photogrammetry particularly advantageous in remote study locations or ones where canyon walls or other obstructions make aerial surveying methods impractical.

One of the chief drawbacks to SfM techniques are issues related to the large data sets they generate and the resulting problems with data management and processing time (Lague et al., 2013; Westoby et al., 2012). This study experienced issues with processing time when converting the field data (digital photographs) into a useable DEM. Processing times were commonly more than 12 hours and sometimes close to 24 hours, although the majority of that time is hands off, while the computer processes information with needing user input.

Once a useable DEM had been created, a second challenge regarding the analytic method emerged. Early attempts at data processing using the conventional software suite ArcGIS proved ineffective. I experienced issues with file types that were too large for ArcGIS to work with or that ArcGIS couldn't open. CloudCompare proved to be an efficient alternative, as it was designed to cope with large point cloud data types. Additionally, it is open source software, meaning quicker tool development and more rapid response to technological advances in data acquisition (CloudCompare, 2014). As with any new method, there are concerns regarding its effectiveness and accuracy. I personally experimented with change detection accuracy and processing efficiency as discussed in section 3. Additional, external verification exists in the recent paper by Lague et al., (2013). In it, they describe change occurring at many scales and differentiate between the causes of morphologic change due to the location and nature of the change. It is my opinion that future morphologic studies will benefit from the continued use and development of this processing software.

Future Work and Areas for Improvement

In addition to the technologic issues described in the section above, there were challenges during the field work. Chief among these challenges was proper camera focus. As outlined by Matthews et al., (2008), properly focused pictures are a crucial part of high quality photograph alignment and therefore low error during analysis. I developed two methods for combating this challenge in the field; 1) fixing the focal length of the lens using tape prevented changes during the picture taking step and 2) ensuring that each beach was covered in more photographs than the necessary for the minimum 66% picture overlap called for by Matthews et al., (2008). Evidence of my improvement in technique when taking pictures is readily apparent in DEMs of certain bars at early times where there are data gaps mid bar. See Appendix A, figure 7 for an example of a dense point clouds from time t1.

As discussed earlier in this section, beach #2 and beach #3 both have data missing at some times. Early field work resulted in data for all four beaches assuming I was on the water well before any commercial trips. As the rafting season progressed, beaches #2 and #3 became increasingly popular for overnight trips. As a result, I was unable to capture the occupied beach. Extending the duration of the field work would result in more DEMs, therefore missing DEMs due to a location being occupied would be less important for the study.

Chapter Six: Conclusion

This thesis explores an emerging technique for generating and analyzing high resolution digital elevation models by examining impacts that recreational river users have on river bar morphology on the Browns Canyon section of the Arkansas River during the summer rafting season of 2014. Results of this study show a correlation between recreational river users and beach erosion, most conclusively at beach #4, during the falling limb of the hydrograph. The relative lack of erosion at beach #2 and #3 was also shown to be indicative of a less erodible beach composition and not related to a lack of use. Regardless the cause, bar change during the study period was shown to be dynamic. The benefits of digital photography to comparable methods of data acquisition of a similar quality include lower costs and significantly less equipment. Despite lengthy processing times experienced in this experiment and by others, digital photogrammetry is a viable means of high resolution digital elevation model generation. The workflow presented in this paper offers high resolution DEMs and is of benefit to future research, especially where space and/or money are limited.

References

Barker, Rachel, Lawrence Dixon, and Janet Hooke. 1997. "Use of Terrestrial Photogrammetry for Monitoring and Measuring Bank Erosion." *Earth Surface Processes and Landforms* 22 (13): 1217-1227.

Bird, Stephen, Dan Hogan, and James Schwab. 2010. "Photogrammetric Monitoring of Small Streams under a Riparian Forest Canopy." *Earth Surface Processes and Landforms* 35 (8): 952-970.

Brasington, James and RMA Smart. 2003. "Close Range Digital Photogrammetric Analysis of Experimental Drainage Basin Evolution." *Earth Surface Processes and Landforms* 28 (3): 231-247.

Carbonneau, Patrice E., Stuart N. Lane, and Normand E. Bergeron. 2003. "Cost-Effective Non-Metric Close-Range Digital Photogrammetry and its Application to a Study of Coarse Gravel River Beds." *International Journal of Remote Sensing* 24 (14): 2837-2854.

Chandler, Jim, Peter Ashmore, Chris Paola, Mike Gooch, and Fred Varkaris. 2002. "Monitoring River-Channel Change using Terrestrial Oblique Digital Imagery and Automated Digital Photogrammetry." *Annals of the Association of American Geographers* 92 (4): 631-644.

Clayton, Jordan A. and John Pitlick. 2007. "Spatial and Temporal Variations in Bed Load Transport Intensity in a Gravel Bed River Bend." *Water Resources Research* 43 (2). W02426, doi: 10.1029/2006WR005253.

Coleman, Rosalind. 1981. "Footpath Erosion in the English Lake District." *Applied Geography* 1 (2): 121-131.

Dewitt, Dominick and O'Neill, Michael. 1998. "Effects of Flow Augmentation on Stream Channel Morphology and Riparian Vegetation: Upper Arkansas River Basin, Colorado." *The Society of Wetlands Scientists*. 8 (4), 591 - 607

Evans, R. 1998. "The Erosional Impacts of Grazing Animals." *Progress in Physical Geography* 22 (2): 251-268.

Fonstad, Mark A., James T. Dietrich, Brittany C. Courville, Jennifer L. Jensen, and Patrice E. Carbonneau. 2013. "Topographic Structure from Motion: A New Development in Photogrammetric Measurement." *Earth Surface Processes and Landforms*. 38 (4), 421-430.

Heritage, George L., David J. Milan, Andrew RG Large, and Ian C. Fuller. 2009. "Influence of Survey Strategy and Interpolation Model on DEM Quality." *Geomorphology* 112 (3): 334-344.

Heritage, GL, IC Fuller, ME Charlton, PA Brewer, and DP Passmore. 1998. "CDW Photogrammetry of Low Relief Fluvial Features: Accuracy and Implications for reach-scale Sediment Budgeting." *Earth Surface Processes and Landforms* 23 (13): 1219-1233.

Kaplinski, Matt, Jeff Behan, Joseph E. Hazel, Mark Manone, and Roderic Parnell. 2003. "Evaluation of Campsite Studies in the Colorado River Ecosystem: Analysis and Recommendations for Long Term Monitoring." *Final Report in Fulfillment of CA-00PG-400255-0001*.

Karnuta, Tom. 1995. "Road and Riverside Geology of the Upper Arkansas Valley: Arkansas Headwaters Recreation Area." *Salida, Colo.: Geotechnics*.

Kauffman, J. Boone and William C. Krueger. 1984. "Livestock Impacts on Riparian Ecosystems and Streamside Management Implications... a Review." *Journal of Range Management*. 430-438.

Knighton, David. 1998. *Fluvial Forms and Processes: A New Perspective.* Arnold, Hodder Headline, PLC.

Lague, Dimitri, Nicolas Brodu, and Jérôme Leroux. 2013. "Accurate 3D Comparison of Complex Topography with Terrestrial Laser Scanner: Application to the Rangitikei Canyon (NZ)." *ISPRS Journal of Photogrammetry and Remote Sensing* 82: 10-26.

Lane, SN. 2000. "The Measurement of River Channel Morphology using Digital Photogrammetry." *The Photogrammetric Record* 16 (96): 937-961.

Lane, SN, TD James, and MD Crowell. 2000. "Application of Digital Photogrammetry to Complex Topography for Geomorphological Research." *The Photogrammetric Record* 16 (95): 793-821.

Lane, SN, KS Richards, and JH Chandler. 1993. "Developments in Photogrammetry; the Geomorphological Potential." *Progress in Physical Geography* 17 (3): 306-328.

Leeder, MR and PH Bridges. 1975. "Flow Separation in Meander Bends." 338-339

Leopold, Luna B., M. Gordon Wolman, and John P. Miller. 1964. *Fluvial Processes in Geomorphology*. Courier Dover Publications.

Marcus, W. Andrew and Mark A. Fonstad. 2010. "Remote Sensing of Rivers: The Emergence of a Subdiscipline in the River Sciences." *Earth Surface Processes and Landforms* 35 (15): 1867-1872.

Matthews, NA. 2008. "Aerial and Close-Range Photogrammetric Technology: Providing Resource Documentation, Interpretation, and Preservation." *Technical Note, Bureau of Land Management, Denver, Colorado*.

Milan, David J., George L. Heritage, Andrew RG Large, and Ian C. Fuller. 2011. "Filtering Spatial Error from DEMs: Implications for Morphological Change Estimation." *Geomorphology* 125 (1): 160-171.

Morgan, RPC and AJ Smith. 1980. "Simulation of Soil Erosion Induced by Human Trampling." *Journal of Environmental Management* 10: 155-165.

O'Brian, G., Janssen, J., Thompson, K. Burke, K. and A. Potochnik. 1999. "Effects of Continuous High Flows and Daily Fluctuating Flows from Glen Canyon Dam on Grand Canyon Sand Bars, 1997 and 1998: A Continuation of Repeat Photography Study by Grand Canyon River Guides, Inc. (Adopt-a-Sand Bar Program)". Administrative Report Submitted by the Grand Canyon River Guides Adopt-a-Sand Bar Program.

O'Brien, G., Burke, K., Hamilton, L. 2000. "Effects of Natural Flow and Controlled-Flow Releases from Glen Canyon Dam on Grand Canyon Sand Bars, 1999: A Continuation of a Repeat Photography Study the Grand Canyon River Guides, Inc. (Adopt-a-Sand Bar Program)". Administrative Report Submitted to the Grand Canyon Monitoring and Research Center by the Grand Canyon River Guides Adopt-a-Sand Bar Program.

Petts, Geoffrey E. 1984. *Impounded Rivers: Perspectives for Ecological Management.* John Wiley.

Powell, D. Mark. 1998. "Patterns and Processes of Sediment Sorting in Gravel-Bed Rivers." *Progress in Physical Geography* 22 (1): 1-32.

Robert, Andre. 2011. "Flow Resistance in Alluvial Channels." *Progress in Physical Geography* 35 (6): 765-781.

Rubin, David M., John C. Schmidt, and Johnnie N. Moore. 1990. "Origin, Structure, and Evolution of a Reattachment Bar, Colorado River, Grand Canyon, Arizona." *Journal of Sedimentary Research* 60 (6): 982-991.

Thompson, K. 2001. "Effects of Low Steady Summer Flows on Grand Canyon Camping Sand Bars, 2000." Report to the Grand Canyon Monitoring and Research Center.

———. 2002. "Long Term Monitoring of Camping Beaches in Grand Canyon: A Summary of Results from 1996-2001." Report to Grand Canyon Monitoring and Research Center.

Thompson, K., Burke, K., Potochnik, A. 1997. "Effects of the Sand Bar-Habitat Building Flow and Subsequent Interim Flows from Geln Canyon Dam on Grand Canyon Camping Sand Bars, 1996: A Repeat Photography Study by Grand Canyon River Guides Adopt-a-Sand Bar Program." Report to the Grand Canyon Monitoring and Research Center.

Tomczyk, Aleksandra M. and Marek Ewertowski. 2012. "Quantifying Short-Term Surface Changes on Recreational Trails: The use of Topographic Surveys and 'Digital Elevation Models of Differences' (DODs)." *Geomorphology*. 183: 58-72.

Trimble, Satanley W. 1994. "Erosional Effects of Cattle on Streambanks in Tennessee, USA." *Earth Surface Processes and Landforms* 19 (5): 451-464.

Tweto, Ogden. 1979. "The Rio Grande Rift System in Colorado". American Geophysical Union, Washington, D.C., Pg 33-56.

Van Alstine, R.E. 1969. "Geology and Mineral Deposits of the Poncha Springs NE Quadrangle, Chaffee County, Colorado." *U.S. Geological Survey Professional Paper 626. 52 p.*

Vincent, Kirk R. and E. D. Andrews. 2008. "Depositional Settings of Sand Beaches along Whitewater Rivers." *River Research and Applications* 24 (6): 771-788.

Westoby, M.J., Brasington, J., Glasser, N.F., Hambrey, M.J., Reynolds, J.M. 2012. "'Structure-from-Motion' Photogrammetry: A Low-Cost, Effective Tool for Geoscience Applications." *Geomorphology*. 179: 300-314.

Wheaton, Joseph M., James Brasington, Stephen E. Darby, and David A. Sear. 2010. "Accounting for Uncertainty in DEMs from Repeat Topographic Surveys: Improved Sediment Budgets." *Earth Surface Processes and Landforms* 35 (2): 136-156.

Appendix A

Figure 1

White nail head as ground control point. Dime for scale.

Figure 2

Scale bar. Approximately 1.2 meters across. The four circular patters are the unique coded markers.

Table 1

Beach #1

			Sample			
weight (g)	1	2	3	4	5	6
wet	175	178.2	176.6	178.8	178.7	178.5
dry	140.5	159.2	168.7	152.7	155.9	154.8
Sieve Size (mm)	Weight (larger than) (g)					
5.60	6.00	44.90	9.40	8.60	18.70	7.30
4.00	6.30	12.60	7.80	2.30	6.90	3.70
2.80	10.80	10.80	12.70	2.50	7.90	1.40
2.00	7.80	10.20	20.60	4.10	6.90	1.60
1.00	11.70	21.00	48.90	69.40	8.10	1.90
0.50	11.60	18.30	41.00	46.30	11.70	5.50
0.15	62.40	32.20	24.80	15.10	80.90	90.10
less than 0.15	15.00	11.20	2.60	1.50	20.80	43.10
	Percentage Above					
Sieve Size (mm)						
5.60	4.3%	28.2%	5.6%	5.6%	12.0%	4.7%
4.00	4.5%	7.9%	4.6%	1.5%	4.4%	2.4%
2.80	7.7%	6.8%	7.5%	1.6%	5.1%	0.9%
2.00	5.6%	6.4%	12.2%	2.7%	4.4%	1.0%
1.00	8.3%	13.2%	29.0%	45.4%	5.2%	1.2%
0.50	8.3%	11.5%	24.3%	30.3%	7.5%	3.6%
0.15	44.4%	20.2%	14.7%	9.9%	51.9%	58.2%
less than 0.15	10.7%	7.0%	1.5%	1.0%	13.3%	27.8%

Beach #2

			Sample			
weight (g)	1	2	3	4	5	6
wet	103	183.9	105.5	178.5	174.8	182.2
dry	86.7	160.7	102.6	152.3	155	164.7
Sieve Size (mm)	Weight (larger than) (g)					
5.60	2.50	2.50	0.00	0.40	7.20	2.30
4.00	0.70	2.50	0.00	0.20	2.20	1.30
2.80	0.40	0.40	0.20	0.70	1.20	1.50
2.00	0.20	0.20	0.20	0.50	1.60	1.10
1.00	0.40	2.30	0.40	0.80	2.40	2.40
0.50	0.70	14.40	1.40	1.60	2.90	4.80
0.15	69.00	89.20	76.10	85.50	109.50	111.20
less than 0.15	12.40	46.60	20.80	61.70	26.20	38.00
	Percentage Above					
Sieve Size (mm)						
5.60	2.9%	1.6%	0.0%	0.3%	4.6%	1.4%
4.00	0.8%	1.6%	0.0%	0.1%	1.4%	0.8%
2.80	0.5%	0.2%	0.2%	0.5%	0.8%	0.9%
2.00	0.2%	0.1%	0.2%	0.3%	1.0%	0.7%
1.00	0.5%	1.4%	0.4%	0.5%	1.5%	1.5%
0.50	0.8%	9.0%	1.4%	1.1%	1.9%	2.9%
0.15	79.6%	55.5%	74.2%	56.1%	70.6%	67.5%
less than 0.15	14.3%	29.0%	20.3%	40.5%	16.9%	23.1%

Beach #3

			Sample			
weight (g)	1	2	3	4	5	6
wet	177.7	202.5	183.1	178.6	175.9	190
dry	152.2	184.9	173.5	146.2	162.8	176.1
Sieve Size (mm)	Weight (larger than) (g)					
5.60	22.60	7.60	32.20	0.00	50.30	55.70
4.00	2.30	4.30	4.80	0.00	10.40	7.20
2.80	1.90	7.30	4.60	0.40	10.20	7.50
2.00	2.00	7.60	4.30	0.80	7.40	8.50
1.00	2.80	15.60	7.30	2.70	12.60	21.80
0.50	10.80	21.60	11.70	17.40	15.60	28.40
0.15	93.50	105.10	74.30	112.50	46.60	39.60
less than 0.15	15.30	15.20	33.90	11.50	8.60	7.10
	Percentage Above					
Sieve Size (mm)						
5.60	14.8%	4.1%	18.6%	0.0%	30.9%	31.6%
4.00	1.5%	2.3%	2.8%	0.0%	6.4%	4.1%
2.80	1.2%	3.9%	2.7%	0.3%	6.3%	4.3%
2.00	1.3%	4.1%	2.5%	0.5%	4.5%	4.8%
1.00	1.8%	8.4%	4.2%	1.8%	7.7%	12.4%
0.50	7.1%	11.7%	6.7%	11.9%	9.6%	16.1%
0.15	61.4%	56.8%	42.8%	76.9%	28.6%	22.5%
less than 0.15	10.1%	8.2%	19.5%	7.9%	5.3%	4.0%

Beach #4

			Sample			
weight (g)	1	2	3	4	5	6
wet	172.4	181.3	177.8	187.1	180.4	180.6
dry	154.4	172.9	168	173.7	174.6	173
Sieve Size (mm)	Weight (larger than) (g)					
5.60	28.20	22.70	18.20	98.20	21.30	0.30
4.00	7.70	3.60	4.00	5.90	1.50	0.50
2.80	7.90	5.20	5.30	4.20	2.20	0.10
2.00	9.30	4.20	5.30	4.40	2.50	0.40
1.00	20.60	7.40	11.60	8.10	6.10	1.00
0.50	35.60	48.80	62.60	9.50	43.80	26.20
0.15	40.60	72.40	58.00	33.30	87.70	136.50
less than 0.15	2.80	9.00	1.60	11.10	2.10	9.40
	Percentage Above					
Sieve Size (mm)						
5.60	18.3%	13.1%	10.8%	56.5%	12.2%	0.2%
4.00	5.0%	2.1%	2.4%	3.4%	0.9%	0.3%
2.80	5.1%	3.0%	3.2%	2.4%	1.3%	0.1%
2.00	6.0%	2.4%	3.2%	2.5%	1.4%	0.2%
1.00	13.3%	4.3%	6.9%	4.7%	3.5%	0.6%
0.50	23.1%	28.2%	37.3%	5.5%	25.1%	15.1%
0.15	26.3%	41.9%	34.5%	19.2%	50.2%	78.9%
less than 0.15	1.8%	5.2%	1.0%	6.4%	1.2%	5.4%

Figure 3

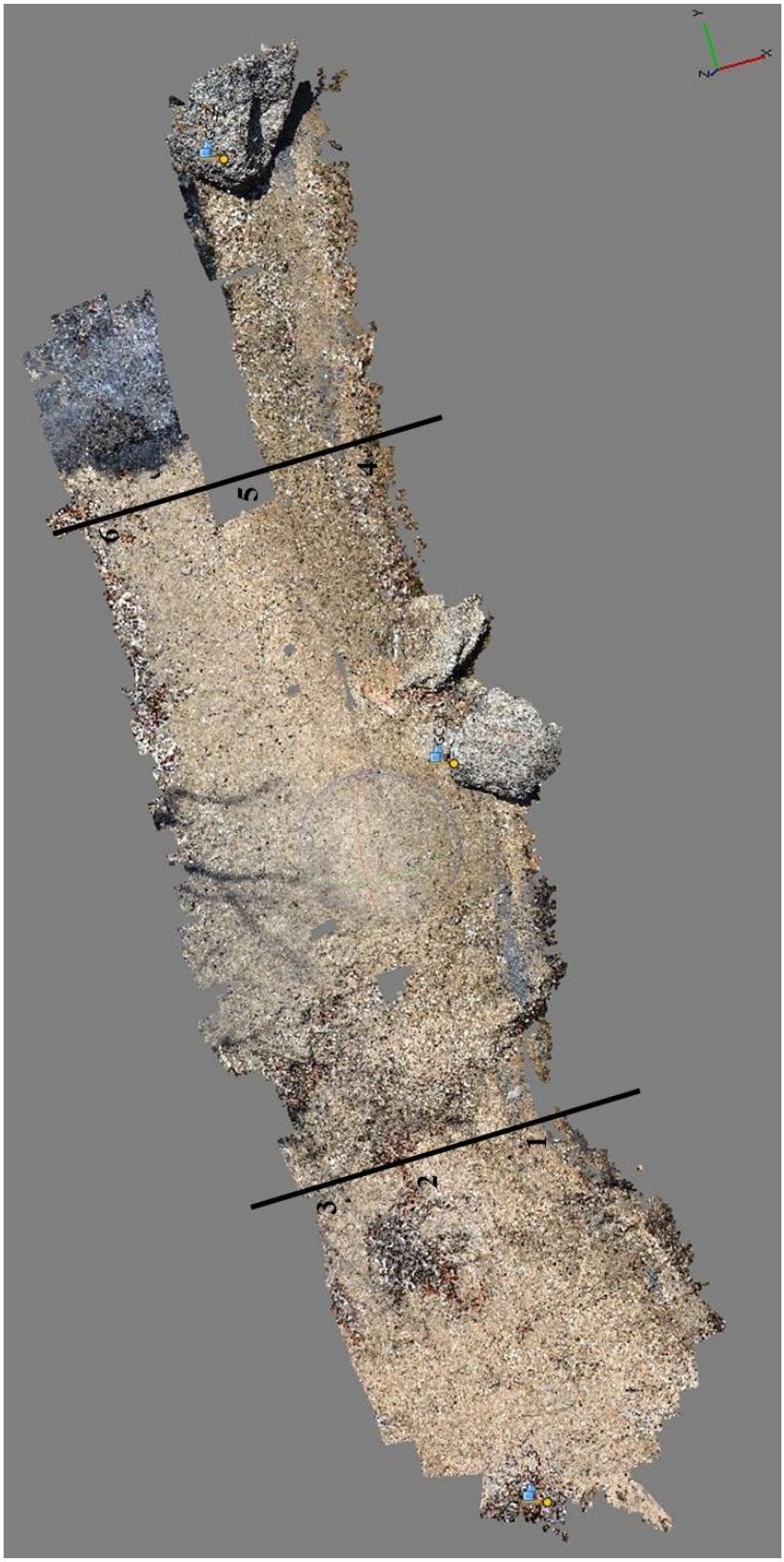

Dense point cloud illustrating beach #1 from time t3. From left to right, ground control points are #3, #1 and #2. The river runs left to right along the bottom of the beach. North is generally to the left.

Figure 4

Dense point cloud illustrating beach #2 from time t7. From left to right, ground control points are #1, #3 and #2. The river runs generally left to right. North towards the upper left corner in this image.

Beach #3, time 3

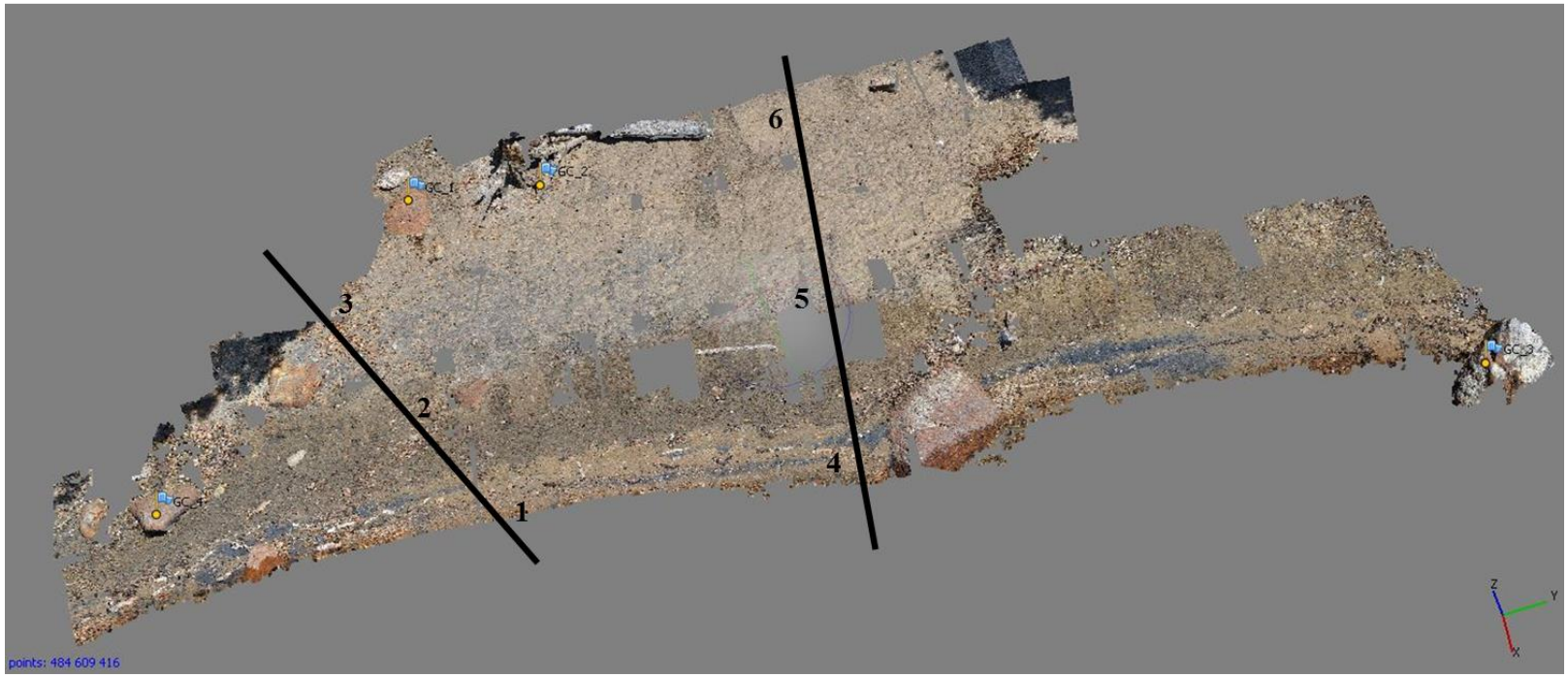

Dense point cloud illustrating beach #3 from time t3. From left to right, ground control points are #4, #1, #2 and #3. The river runs left to right along the bottom of the beach. North is generally to the left.

Figure 6

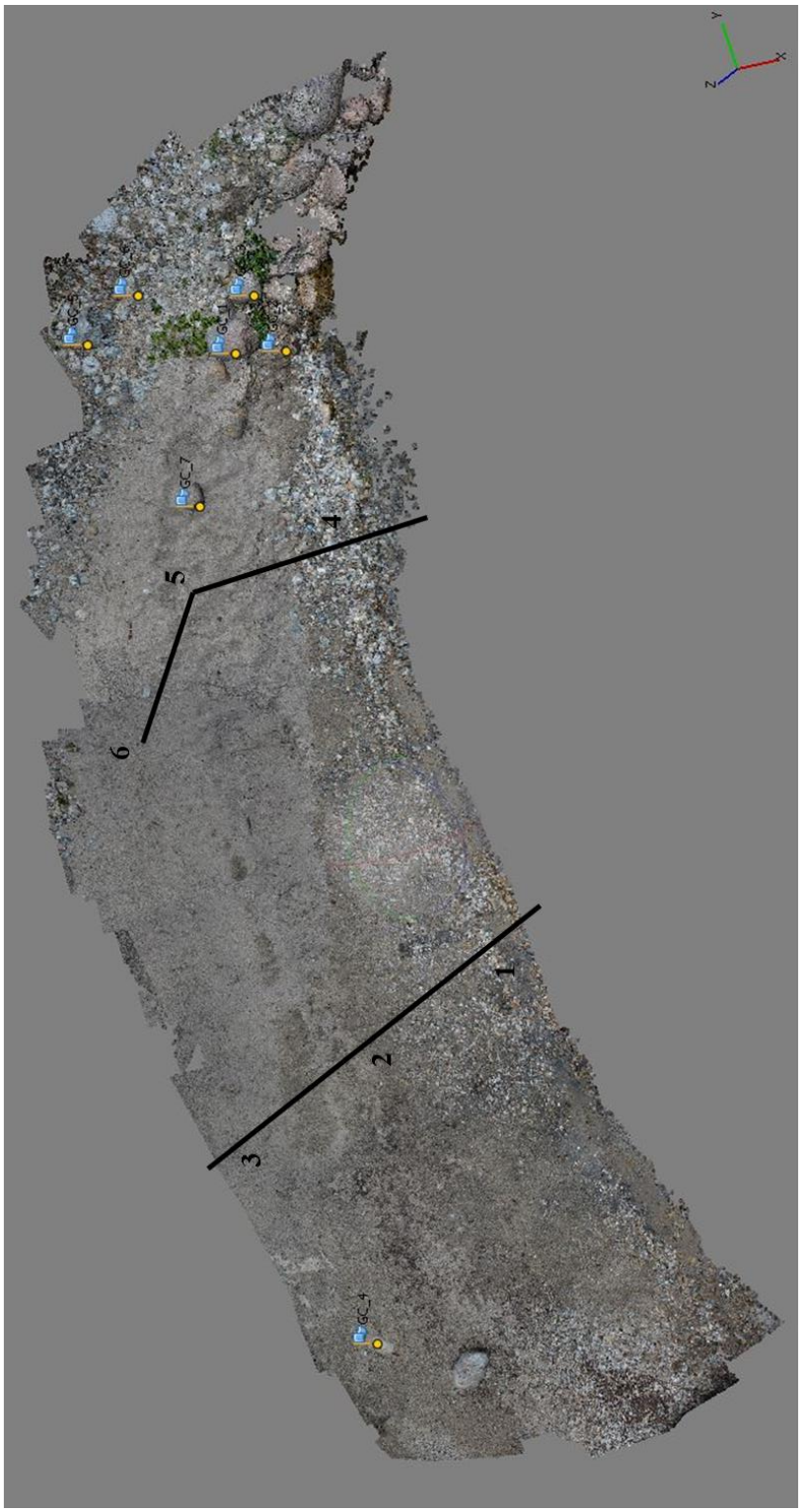

Dense point cloud illustrating beach #4 from time t8. From left to right and clockwise, ground control points are #4, #7, #5, #6, #3, #2 and #1. The river runs top to bottom along the left side of the image, hitting an exposed bedrock cliff and creating a large recirculation zone at the bottom of the image. North is generally up.

Figure 7

Figure 8

Appendix B

Figure 1

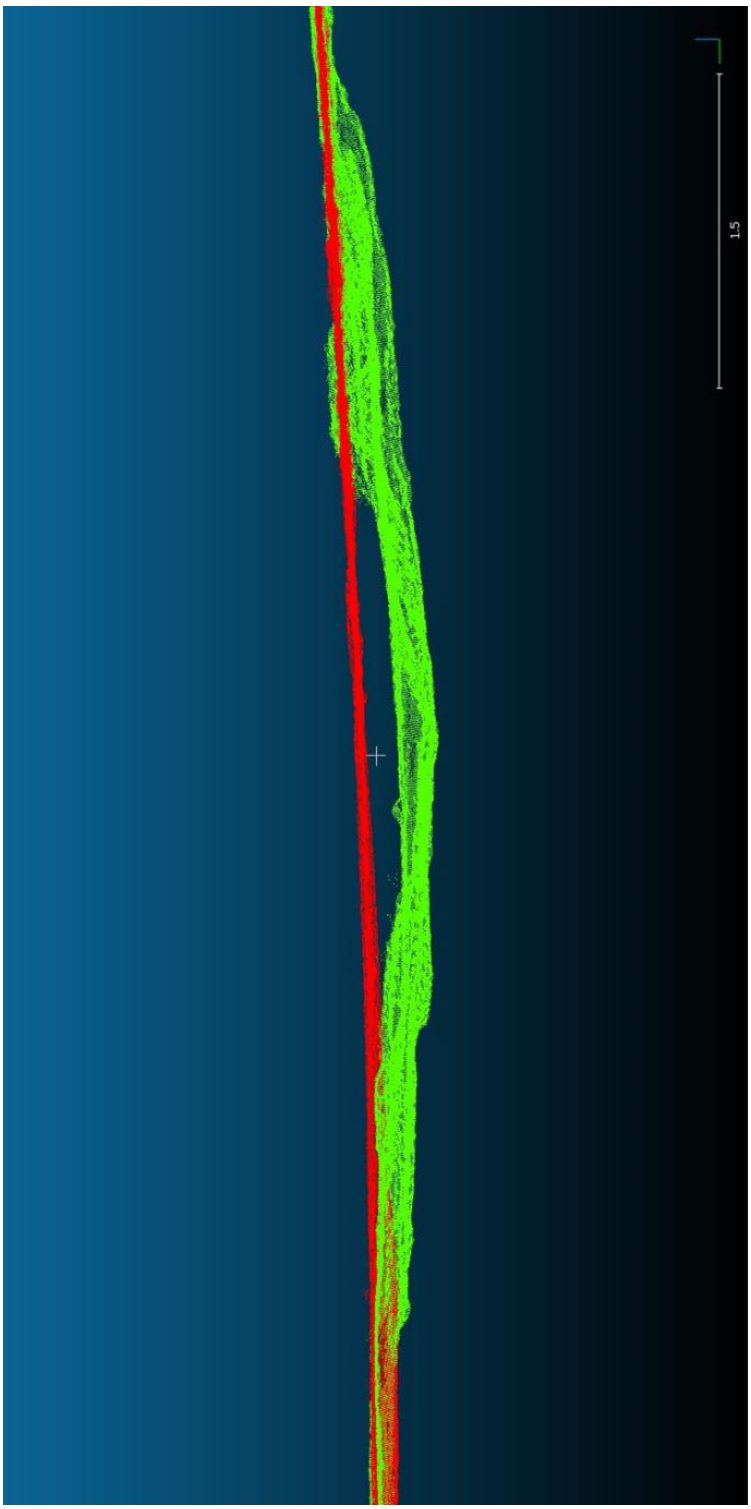

Latitudinal cross section of beach #1, time t3 to t5. Time t3 is green, time t5 is red. The gap between each DEM shows the area where deposition occurred during peak runoff.

Figure 2

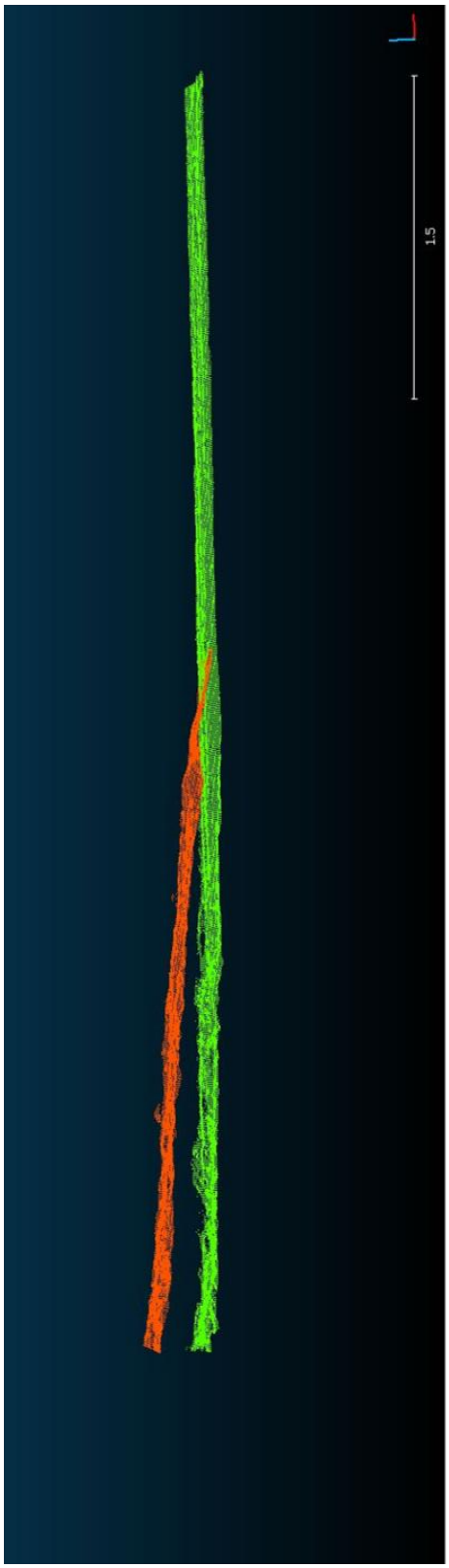

Longitudinal cross section of beach #1, time t7 to t8. Time t7 is orange, time t8 is green. The gap between each DEM shows the area where erosion occurred during the rain event between times t7 and t8.

For all of the following DoDs, north is to the left and the water surface is at the bottom of the image. Grey areas are areas with DoD return of *NoVal*, meaning there was no overlap between the two DEMs.

Figure 3. B1_t2-t3

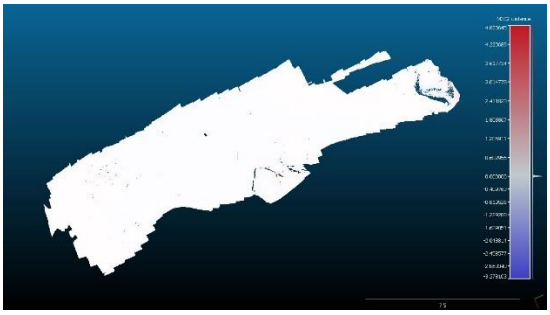

Figure 4. B1_t3-t5

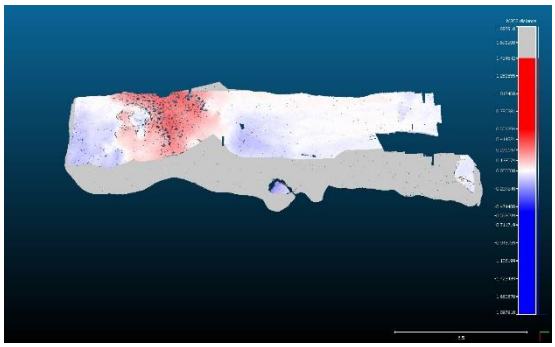

Figure 5. B1_t5-t6

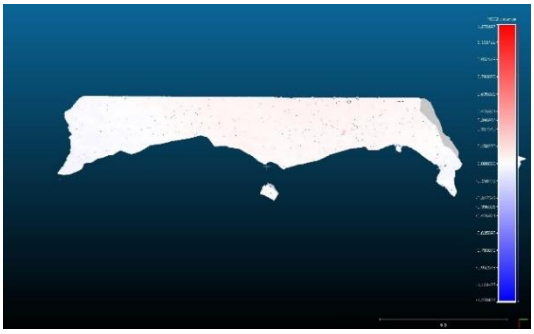

Figure 6. B1_t6-t7

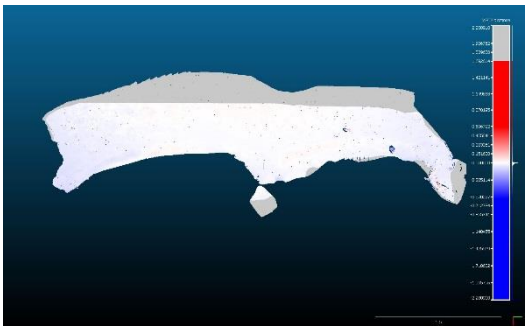

Figure 7. B1_t7-t8

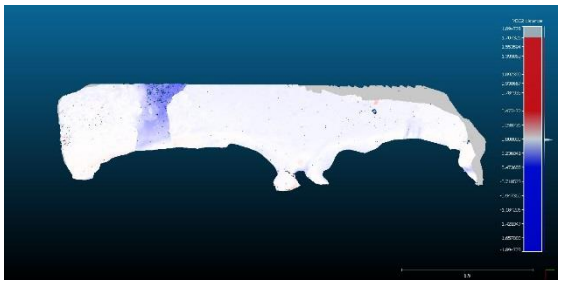

Figure 8. B1_t7-t8

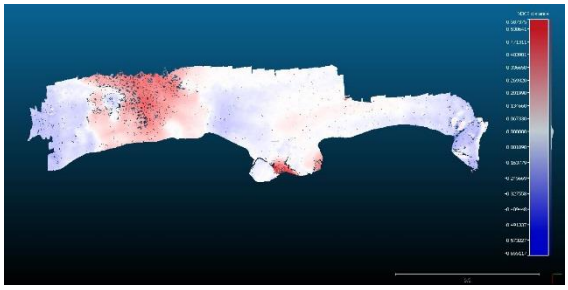

Appendix C

For all of the following DoDs, north is to the left and the water surface is at the bottom of the image. Grey areas are areas with DoD return of *NoVal*, meaning there was no overlap between the two DEMs.

Figure 1. B2_t2-t3

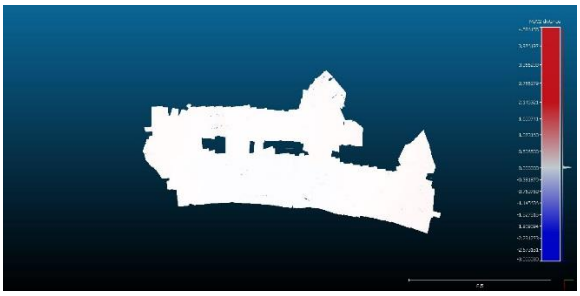

Figure 2. B2_t3-t5

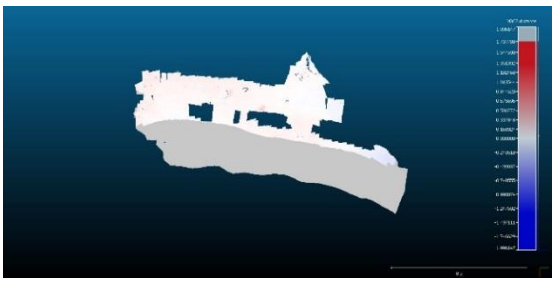

Figure 3. B2_t5-t6

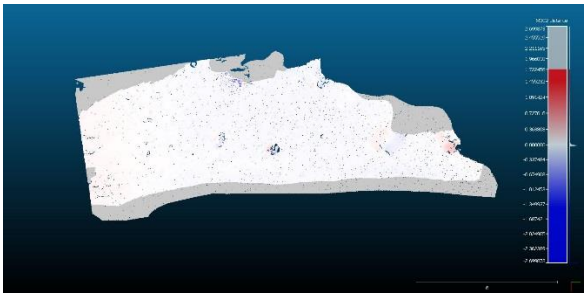

Figure 3. B2_t2-t6

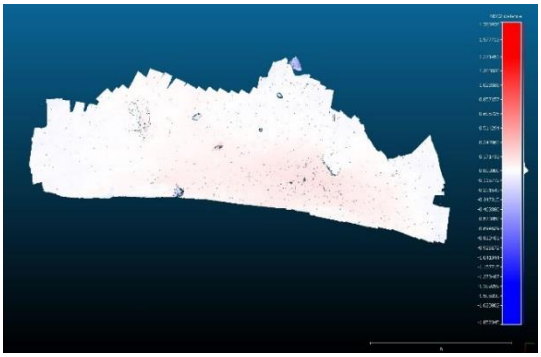

Appendix D

For all of the following DoDs, north is to the left and the water surface is at the bottom of the image. Grey areas are areas with DoD return of *NoVal*, meaning there was no overlap between the two DEMs.

Figure 1. B3_t2-t3

Figure 2. B3_t3-t4

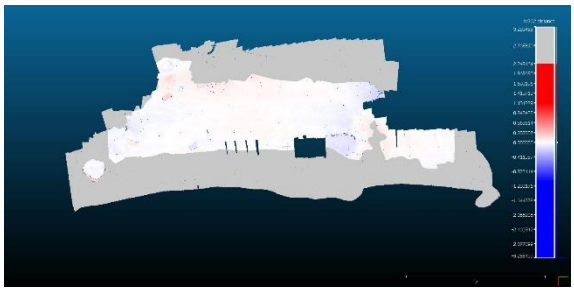

Figure 3. B3_t4-t7

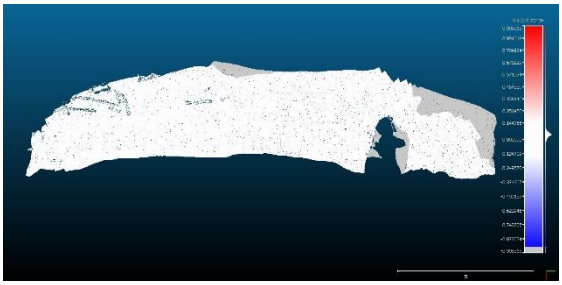

Figure 4. B3_t2-t7

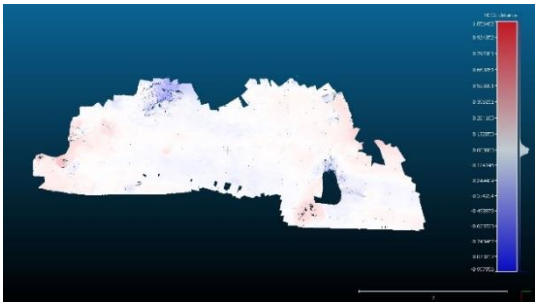

Appendix E

For all of the following DoDs, north is to the left and the water surface is at the bottom of the image. Grey areas are areas with DoD return of *NoVal*, meaning there was no overlap between the two DEMs.

Figure 1

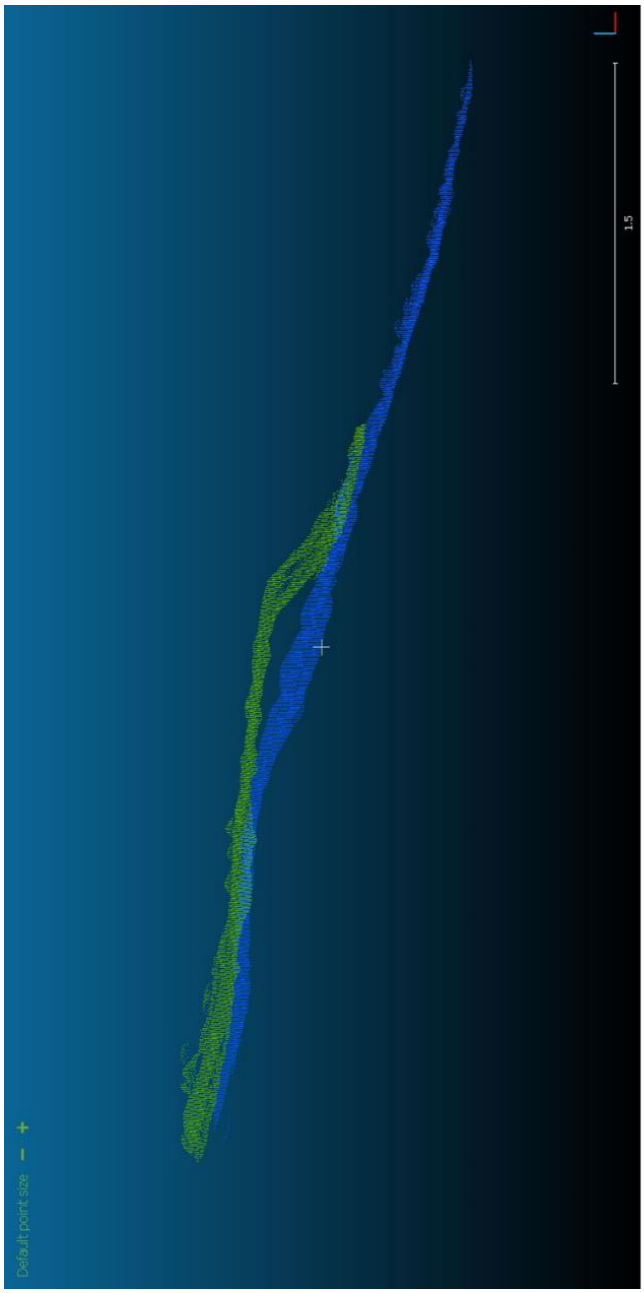

Longitudinal cross section of beach #4, time t6 to t8. Time t6 is green, time t8 is blue. The gap between each DEM shows the area where deposition occurred during peak runoff. Notice the overall flattening of the beach.

Figure 2. B4_t2-t3

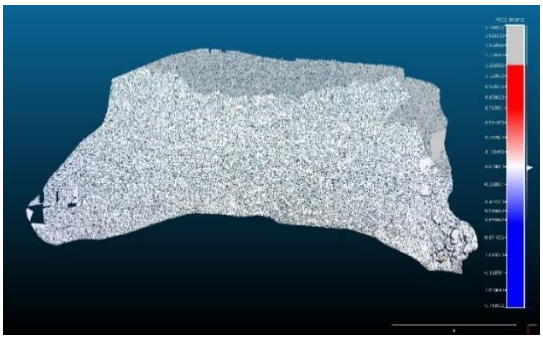

Figure 3. B4_t3-t5

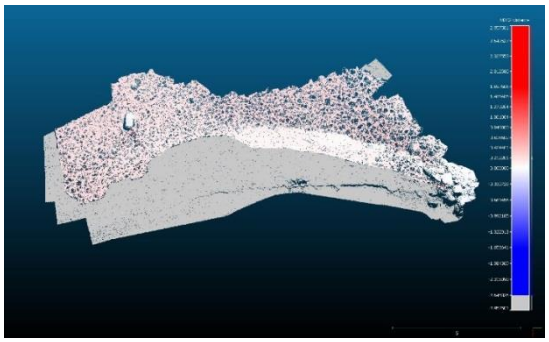

Figure 4. B4_t5-t6

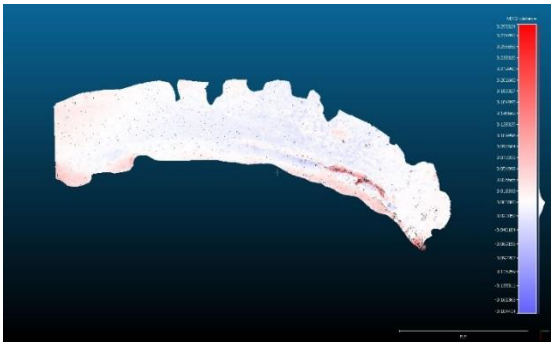

Figure 5. B4_t6-t7

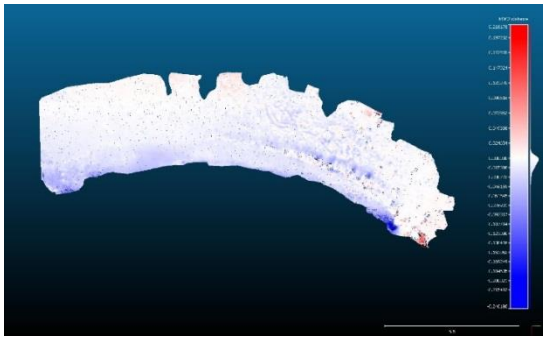

Figure 6. B4_t7-t8

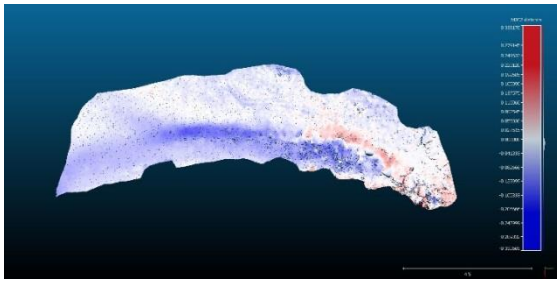

Figure 7. B4_t2-t8